

Study of the Effectiveness of a Laboratory-Scale System to Reduce Water Super-Saturation

Final report to the U.S. Bureau of Reclamation
Water Treatment Engineering and Research
P.O. Box 22007, Department 82-30
Denver CO 80225

ANDREA PROSPERETTI and XU GENG
Department of Mechanical Engineering
The Johns Hopkins University, Baltimore MD 21218, U.S.A.
prosperetti@jhu.edu
xgeng1@jhu.edu

Contents

Abstract	iii
1 Introduction	1
2 Micro-bubble generator	2
3 Bubble size measurement	9
4 Experimental set-up and procedure	14
5 Experimental results	17
6 Bubble growth by diffusion	18
7 Mathematical model and numerical simulation	20
8 Numerical method	23
9 Numerical results	23
10 Conclusions	32
References	35

Abstract

Occasional gas super-saturation of the water in which they live has resulted in large fish kills. A promising way to bring down the dissolved gas concentration is to inject small air bubbles in the water. The bubbles provide surface area across which the dissolved gases can leave the liquid and, with their ascensional motion, they promote convective currents which intensify the renewal of the surface of the water body, through which the gas can return to the atmosphere.

A significant obstacle in the practical application of this technique has been the difficulty of producing effectively and economically the large numbers of small bubbles necessary for this purpose. This study was directed to the investigation of the effectiveness of a novel method to produce such large quantities of small bubbles.

This report describes the experimental procedures and the results of several tests which show that the bubbles produced in this way are very effective at removing dissolved gases. A mathematical model is also developed which proves able to explain the data and to give useful information on the effect of the various parameters of the problem. The bubble size emerges as the most critical feature of an effective system. In particular, it is found that the effectiveness of bubbles rapidly decreases when their radius becomes larger than about 150-200 μm .

This report describes the work undertaken to execute the project described in a proposal by the same title submitted to the U.S. Bureau of Reclamation in late December 2004. The starting date of the project was July 15, 2005.

1 Introduction

The problem addressed in this work is the reduction of super-saturated oxygen and nitrogen concentrations in water bodies.

Research and experience has shown that these super-saturated conditions (and in particular, nitrogen) can result in large fish kills by a process similar to that causing the so-called “bends” in deep-sea divers. Namely, the blood becomes super-saturated, which can lead to the formation and growth of bubbles. The growing bubbles, in turn, can rupture or occlude blood vessels and damage the surrounding tissues and organs.

Flowing water in streams or rivers is usually saturated or slightly super-saturated with air due to turbulence and surface disruption caused by waves, boulders, etc. Saturation is however a decreasing function of temperature. If, therefore, there is a temperature rise, the water will become super-saturated and hazardous conditions may result. The problem is particularly acute for nitrogen, which has a lower solubility than oxygen in water, and which therefore reaches super-saturation conditions more readily.

Such super-saturated conditions may persist for some time if the water flow slows down as in the basin of a dam. The reason is that gas diffusion in liquids is a very slow process so that it takes a long time for the dissolved gases at depth to reach the surface and escape into the atmosphere. Gas at a depth h below the free surface can be expected to diffuse to the surface after a time of the order of h^2/D , where D is the gas diffusivity. Typical values of D are of the order of 10^{-9} m²/s so that the diffusion time over a distance of 1 m would be extremely long if one had to rely on molecular diffusion alone. In practice, there is always some convection which leads to renewal of the surface layer and thus shortens these times considerably. However, even with this mechanism, the persistence times of super-saturated conditions have been found able to reach hazardous levels.

The aim of this project is to speed up the ex-solution of dissolved gases by injecting bubbles into the super-saturated liquid. This approach may appear at first sight counter-intuitive, but is in fact very beneficial for two reasons:

1. In the first place, the bubbles provide surface area across which the dissolved gases can leave the liquid. When the bubbles reach the surface and pop, the dissolved gas is returned to the atmosphere.
2. With their ascensional motion, the bubbles promote convective currents in the water body and thus intensify the surface renewal process mentioned before.

The efficiency of the process depends strongly on the bubble size. A given amount of gas distributed in the form of large bubbles is not very effective as the bubbles rise to the surface quickly and do not provide therefore much time for gas to diffuse into them. The

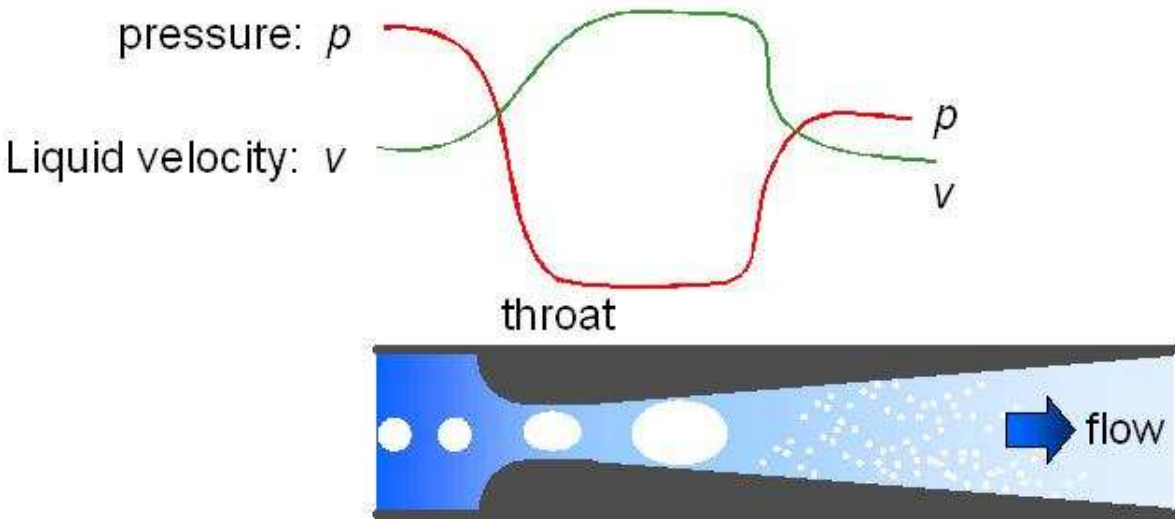


Figure 1: Schematic of the bubbly flow in a converging-diverging nozzle.

same amount of gas provided in the form of smaller bubbles is better insofar as it provides a large surface area and long residence time. However, if the bubble radius is too small, the bubbles may either shrink due to the effect of surface tension – thus leading to an *increase* in gas content of the liquid – or rise so slowly as to have a negligible effect, especially on promoting convection.

The size of the bubbles is therefore a key parameter in the design of an effective and efficient system. A desirable size is of the order of a few hundred micrometers, which presents a serious practical problem as it is difficult and energetically expensive to produce large quantities of bubbles in this size range. The use of porous plates is undesirable due to clogging. Mechanical means to break up gas volumes are inefficient because the energy that eventually is made available at the $100\ \mu\text{m}$ -scale-range to form bubbles of the desired size is typically only a small fraction of the mechanical energy input to the system.

In this work we study the effectiveness a new way to produce small bubbles. Furthermore, we have developed a simplified mathematical model which provides a good explanation of the laboratory data and gives some useful insights into the effect of the various parameters of the system.

2 Micro-bubble generator

The micro-bubble generator used in these experiments is based on a novel concept developed at the University of Tokyo in Prof. Matsumoto's group (Fujiwara et al. 2004). The idea is to flow a liquid containing relatively large bubbles (a few millimeters in diameter) through a converging-diverging Venturi nozzle. As it flows through the nozzle, the liquid velocity

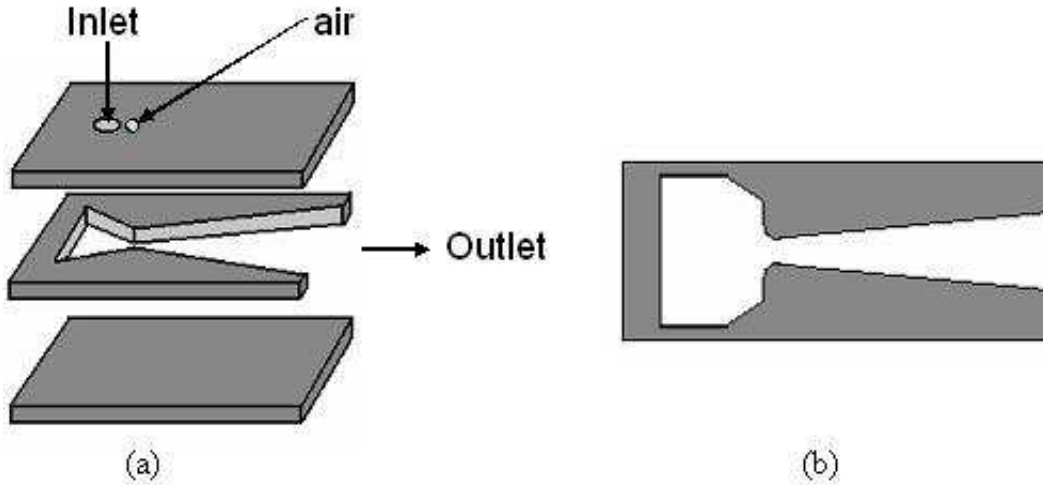


Figure 2: Construction of the nozzle used in the present experiments

increases, while the pressure drops to its lowest level in the neighborhood of the throat. The gas is drawn into the liquid due to the pressure fall in the converging part thus obviating the need for an active pumping action. The pressure recovery in the diverging part causes these entrained bubbles to collapse violently breaking up into small fragments as a result. A schematic of the flow situation in the nozzle is shown in Figure 1.

The great advantage of this method is that the diameter of the nozzle can be orders of magnitude larger than the desired bubble diameter, thus avoiding the clogging problems that plague the use of porous plates, frit disks and the like. At the same time, mechanical energy is supplied directly at small spatial scales and it is therefore employed very efficiently. A downside is that a relatively high liquid velocity at the throat is required for an effective bubble break-up, with an attendant pressure loss.

The bubble fragmentation process may be aided by local cavitation in the nozzle, which is all the more likely if, as in the case of present experiments, the water is super-saturated with air. On the one hand, air super-saturation facilitates the formation of bubbles by cavitation. On the other, the dissolved air diffuses into the cavitation bubbles with the result that, when the pressure recovers and the cavitation bubbles collapse and shatter, they leave behind very small gas bubbles.

In our study nozzles were made by stacking together three acrylic plates (Figure 2a), each with a thickness of 1.5 mm. The middle one (Figure 2b) is cut so as to form the converging-diverging shape of the nozzle. The slope of the diverging part has to be small to avoid flow separation and the attendant large pressure drop. For axisymmetric shapes with a length over diameter ratio of 15, it is recommended that the angle be kept below about 8° (see e.g. Blevins 1984), while for two-dimensional diffusers with the same aspect

ratio the limit is lower, about 6° . We chose 6° on the basis of several tests which monitored the extent of the cavitation zone downstream of the throat. We found that cavitation appeared more readily and was more extended for angles of around 5 to 6° .

A water inlet port is opened in the upper plate, which also contains the air intake port in correspondence of the throat on the nozzle. As noted before, since the pressure is low near the throat, there is no need to have an air compressor to inject air into the nozzle. A valve is connected to the air intake port to control the air flow rate into the nozzle.

The geometric parameters of the nozzle used in our experiments are the following:

- throat width 2 mm
- outlet width 7 mm
- length of the diverging part 30 mm
- thickness of the middle plate 1.5 mm
- throat area 3 mm^2
- water inlet port inner diameter 4 mm
- air inlet port inner diameter 0.3 mm

A typical snapshot of the flow of a bubbly liquid through one of our nozzles is shown in Figure 3. Here the water flow rate was 2.4 l/min, which resulted in a velocity of approximately 13 m/s at the throat, and the gas flow rate was measured to be 12 ml/min.

A similar snapshot for a situation in which there was no gas injection, but bubbles were formed by cavitation, is shown in Figure 4. To promote cavitation it was necessary to increase the water flow rate which in this case was 3.6 l/min, corresponding to about 20 m/s liquid velocity at the throat. The higher liquid velocity induces a large pressure drop, which results in cavitation incipience just after the throat. Vapor bubbles continue to grow downstream of the throat by inertia and by absorbing air from the surrounding water by diffusion reaching a large size. Their collapse downstream of the throat generates many micro bubbles.

Two details of Figure 3 at two successive locations downstream of the throat are shown in Figure 5. These images can be compared with similar ones taken at 1/3 of the gas flow rate, 4 ml/min, shown in Figure 6. The reduction of the gas flow rate leads to a decrease of the number of bubbles but also, more importantly, to smaller bubbles.

Similar enlargements of Figure 4 for the cavitating case are shown in Figure 7. It is evident that, while energetically more expensive due to the need for a higher velocity, cavitation produces much smaller bubbles which, as shown later in Figure 14, are very effective in removing the dissolved gases.

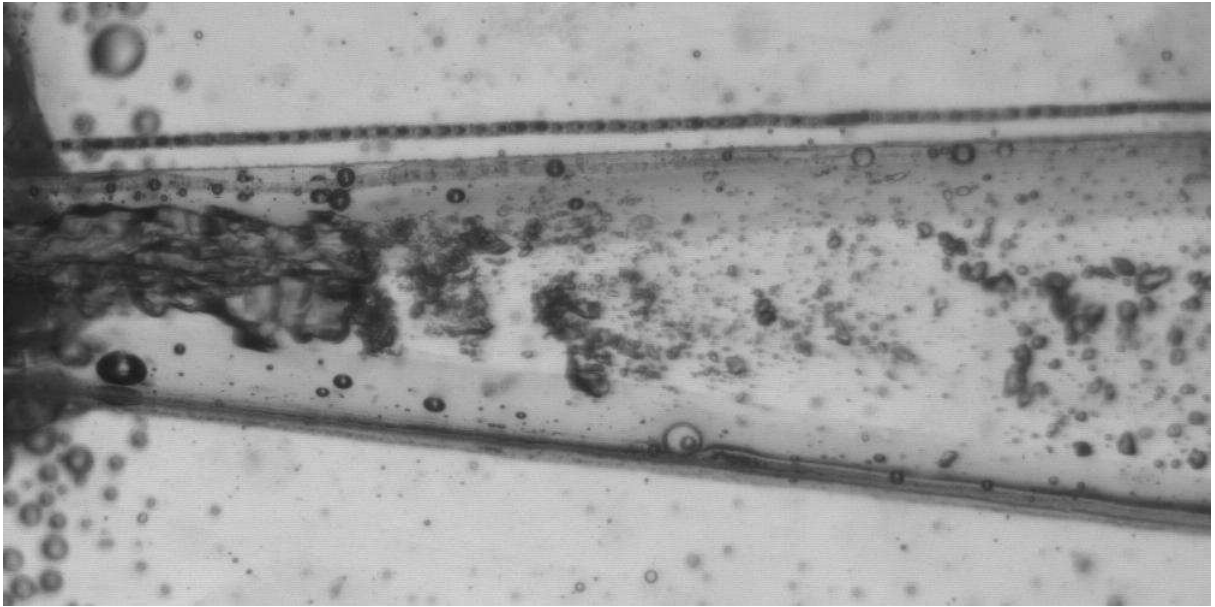


Figure 3: Gas bubble flow in the nozzle. The water flow rate is 2.4 l/min, which resulted in a velocity of 13 m/s at the throat, and the gas flow rate was measured to be 12 ml/min.

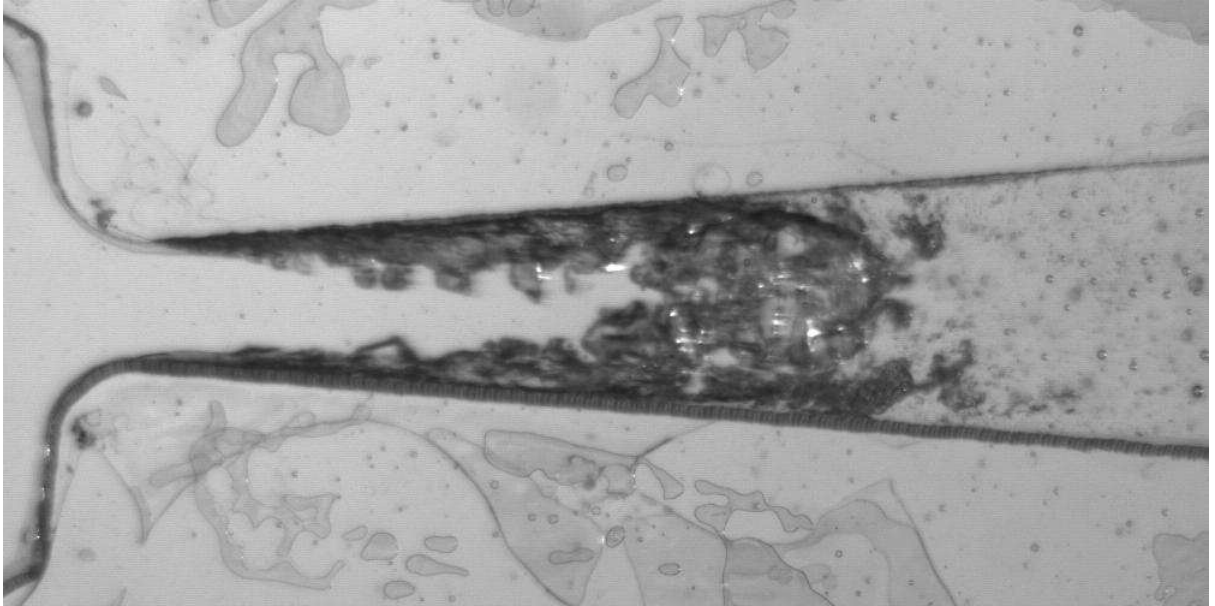


Figure 4: Cavitating flow in the nozzle. The water flow rate is 3.6 l/min, corresponding to a 20 m/s liquid velocity at the throat.

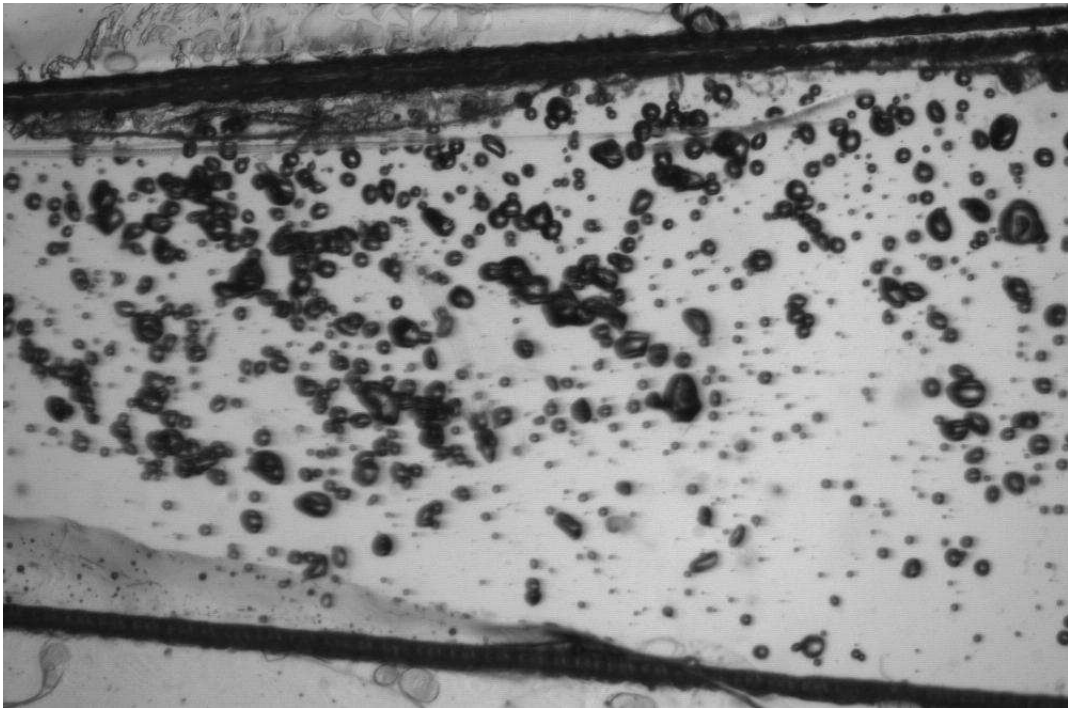
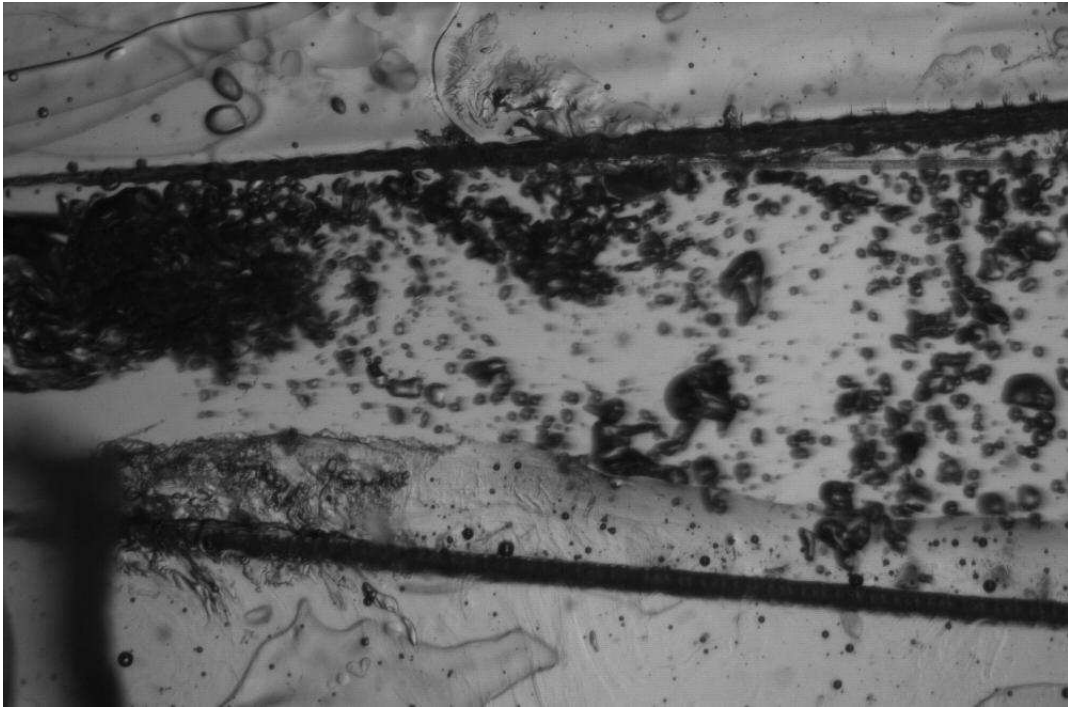


Figure 5: Details of Figure 3 at two successive locations downstream of the throat. The water flow rate is 2.4 l/min and the gas flow rate 12 ml/min.

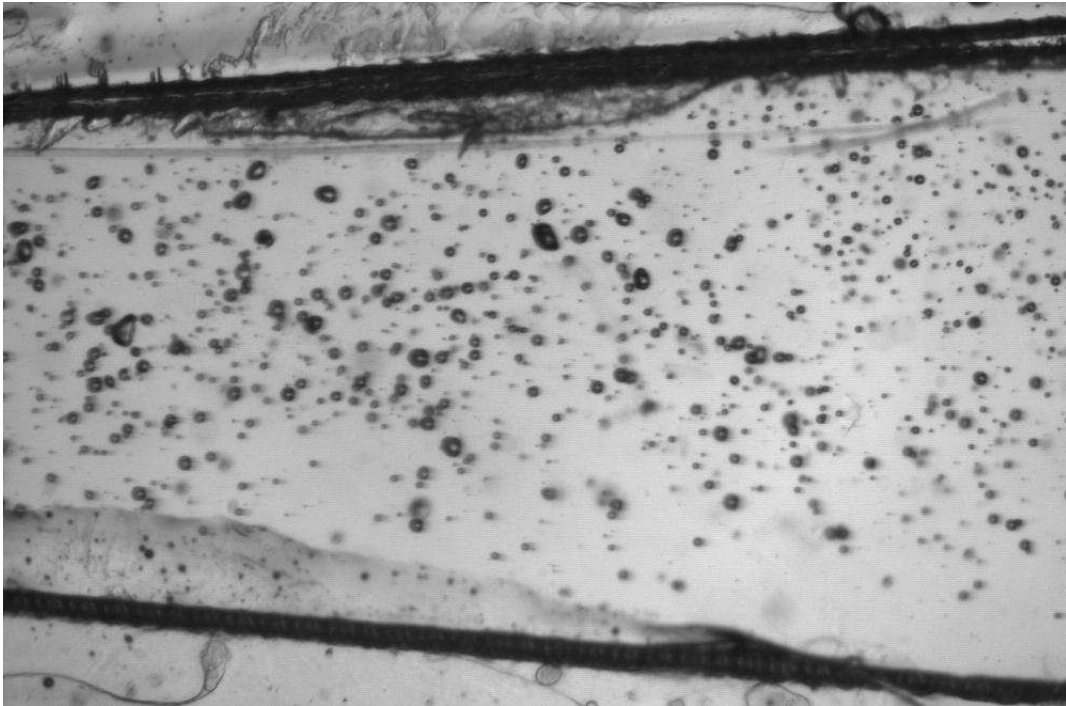
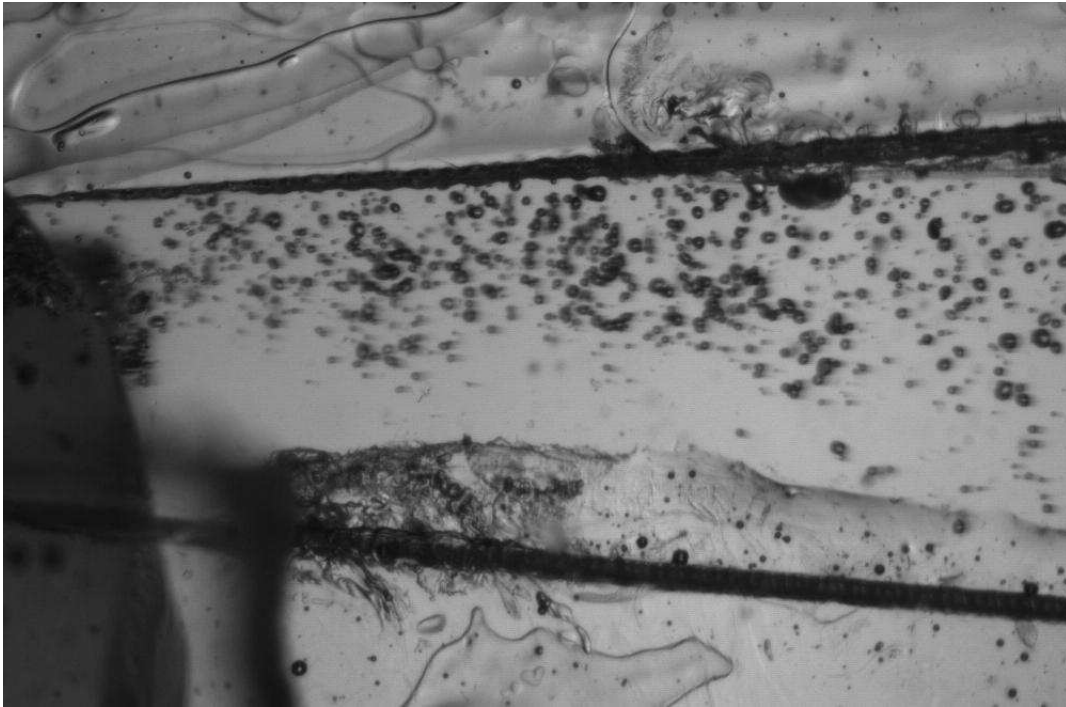


Figure 6: Details of a gas bubble flow similar to that of Figure 3 at two successive locations downstream of the throat. The water flow rate is 2.4 l/min and the gas flow rate 4 ml/min.

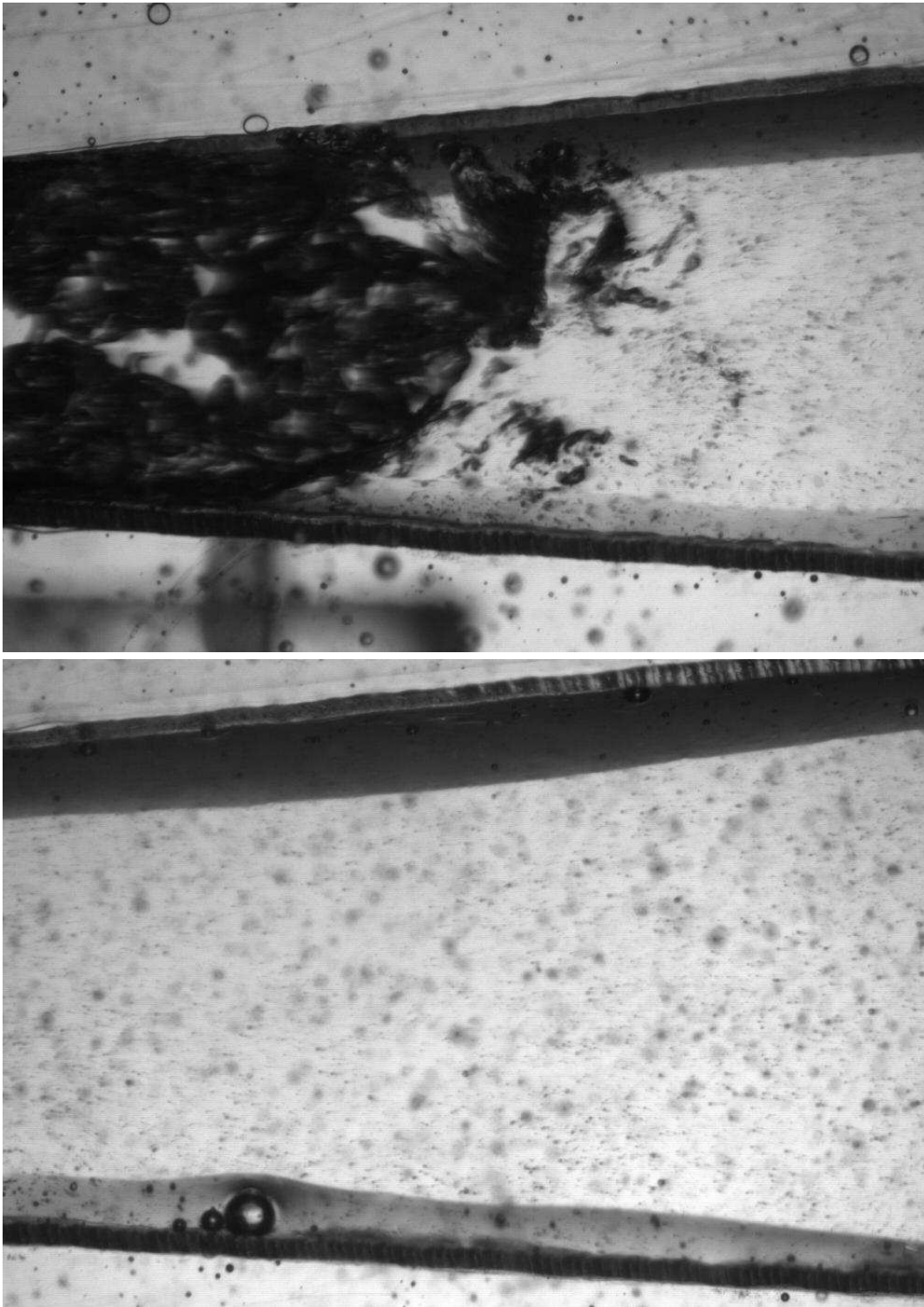


Figure 7: Details of the cavitating flow of Figure 4 at two successive locations downstream of the throat. The water flow rate is 3.6 l/min.

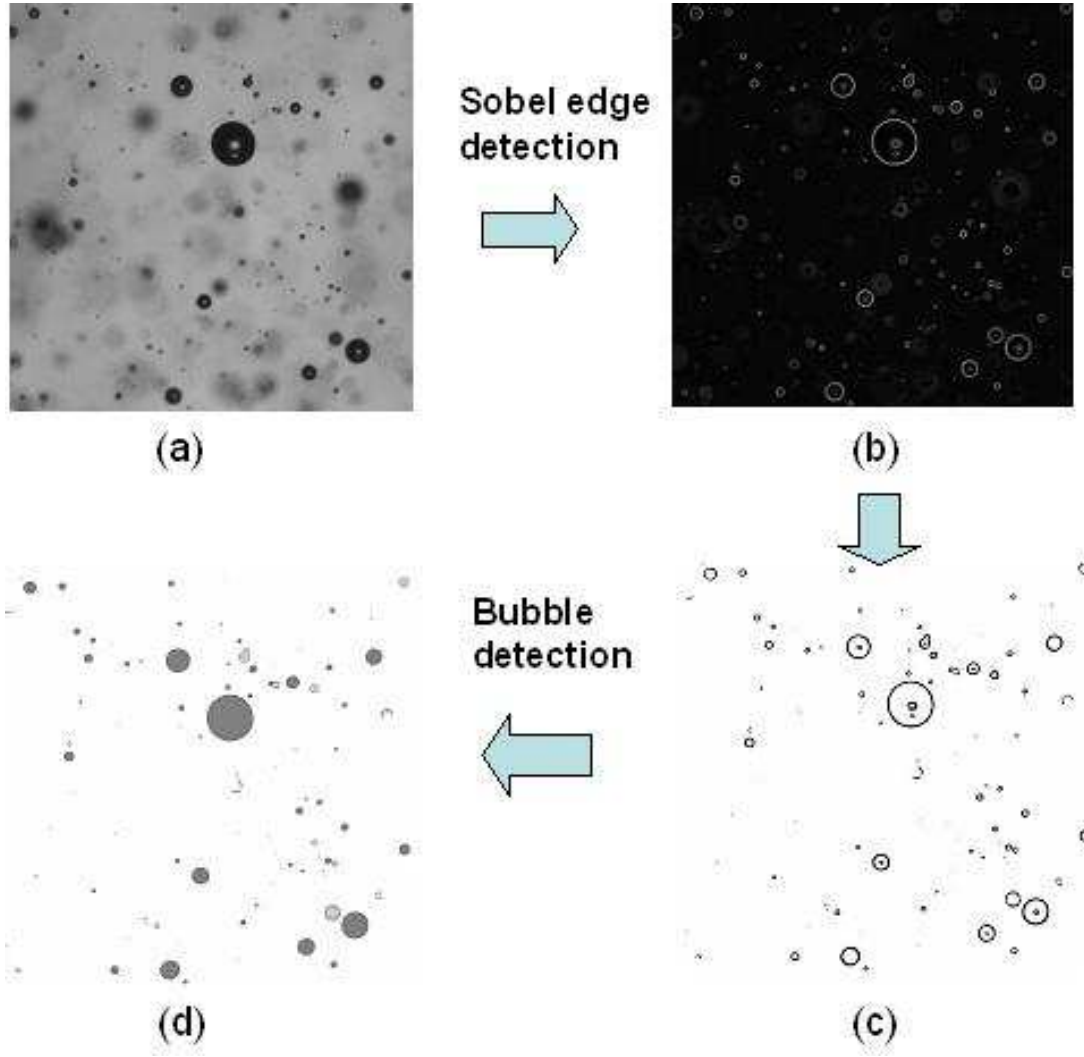


Figure 8: Illustration of the procedure used to measure the bubble size. The CCD camera images (a, upper left) first passed through a Sobel edge-detection algorithm (b, upper right), and then threshold-filtered (c, lower right). The resulting images are scanned to identify transitions from white to black and vice-versa, and individual bubble shapes are obtained as a stream of x and y values.

3 Bubble size measurement

In view of the critical role played by the bubble size in the process under investigation, it was felt necessary to obtain a quantitative measure of the probability distribution of this quantity.

Bubble size measurements were obtained by means of a CCD camera (OpSci Vision

System) following a procedure developed by Oğuz (1998). The bubbler was attached to the bottom of a glass tank filled with tap water. The camera's resolution was set at at $3 \mu\text{m}/\text{pixel}$ which, although not the highest magnification available, permitted us to have a window large enough to obtain a suitably large number of bubbles. Illumination was provided by a $6 \mu\text{s}$ strobe (EGG MV1000) placed facing the camera. A 4 mm-thick white plastic screen used as a diffuser between the strobe and the camera provided adequate lighting. The bubble images were captured 50 mm downstream from the outlet of the nozzle. The sequence of steps of the image processing algorithm is depicted in Figure 8. The images (Figure 8a) are first passed through a Sobel edge-detection algorithm (Figure 8b), followed by a threshold filter (Figure 8c). This procedure eliminates most off-focus bubbles, and only sharp edges of original images are left in the resulting black/white images. Then by scanning these images to track the transition from white to black and vice-versa, individual bubble shapes are obtained as a stream of x and y values. Overlapping bubbles generally contain high curvatures along the boundary. The boundary of bubbles off-focus is not smooth and large deviations of the local curvature relative to the average radius can also be found for them. Therefore, a curvature test will eliminate overlapping bubbles and off-focus bubbles. Once a candidate bubble shape passes these tests, its area is computed in terms of number of pixels. The bubble radius is then computed as the radius of a circle having the same area. Circles filled with a dark color in Figure 8d are the bubbles finally detected.

Typical bubble size distributions for gas flow rates of 4 ml/min and 8 ml/min are shown in figure 9 corresponding to a water flow rate 2.4 l/min. The histograms are the bubble size distributions based on 300 images and 5000 bubbles. The dashed line is a fit to the data as a log-normal distribution

$$PDF(R) = \frac{\exp\{-[\log((R - \theta)/m)]^2/(2\sigma^2)\}}{\sqrt{2\pi}\sigma(R - \theta)} \quad R \geq \theta \quad (1)$$

where m is the scale parameter, σ the shape parameter, and θ the location parameter. For the curve shown in the upper Figure 9 $m = 20 \mu\text{m}$, $\sigma = 0.68$ and $\theta = 0$, while for the lower figure $m = 18 \mu\text{m}$, $\sigma = 0.70$ and $\theta = 0$. For both cases, the peak of the curve is around $10 \mu\text{m}$, and most of the bubbles have a radius less than $50 \mu\text{m}$. The results for the higher gas flow rate, 8 ml/min, are very close to those for the previous case, 4 ml/min, which would imply that the bubble numbers are approximately doubled. Actually, this conclusion neglects the larger bubbles which contain an appreciable amount of gas, but are not present in sufficient number for meaningful statistics. Figure 10 shows the measured size spectrum in the large-radius region. It is seen here that most of the additional gas for the 8 ml/min case goes to form large bubbles for which the fit (1) gives a poor representation.

The origin of this increased number of large bubbles at the higher flow rate is not clear at this stage. It may well be that their appearance is a consequence of coalescence of smaller bubbles, which becomes more likely as the bubble number density increases, given that it depends quadratically on this quantity. In a natural environment bubble coalescence would probably be inhibited by the many impurities suspended in the water. This mechanism

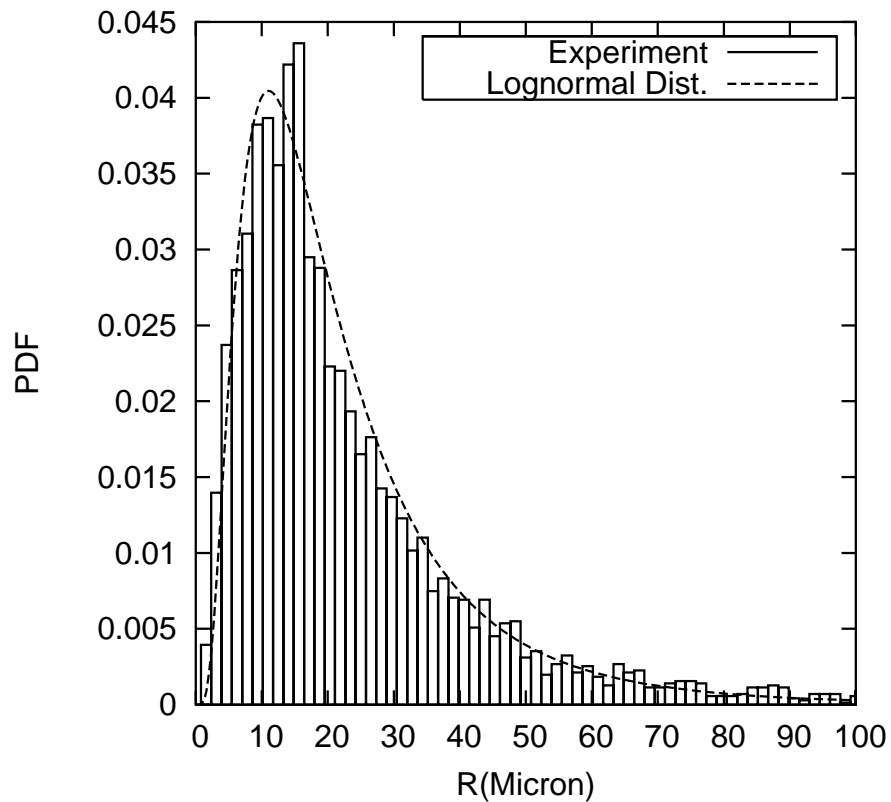
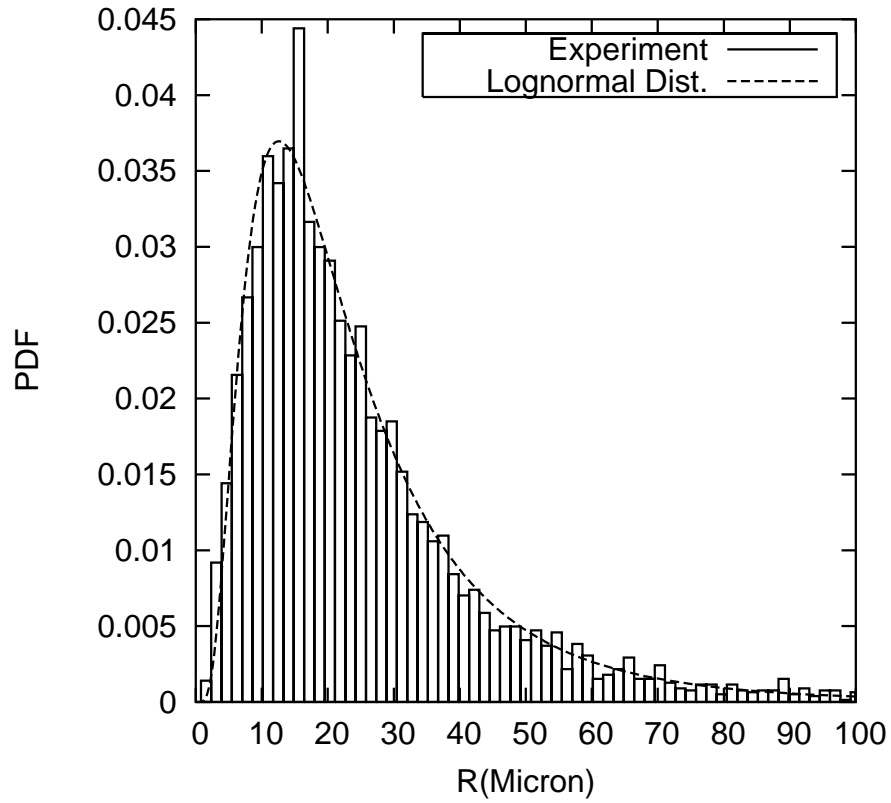


Figure 9: Measured bubble size distribution for gas flow rates of 4 ml/min (top) and 8 ml/min; the water flow rate was 2.4 l/min. The dashed lines are fitted log-normal distributions.

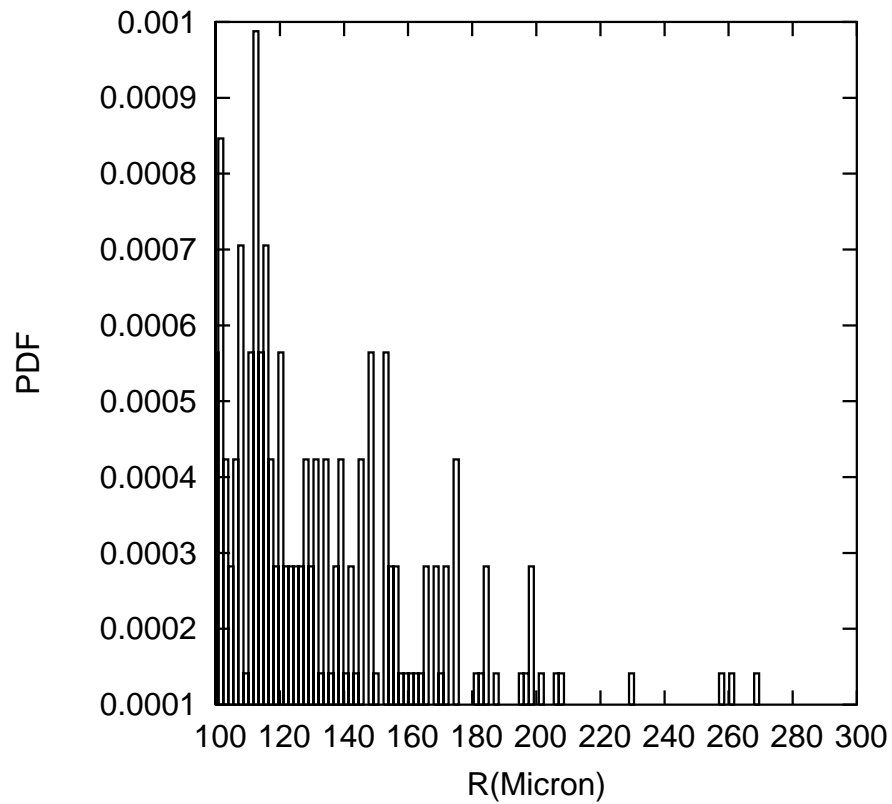
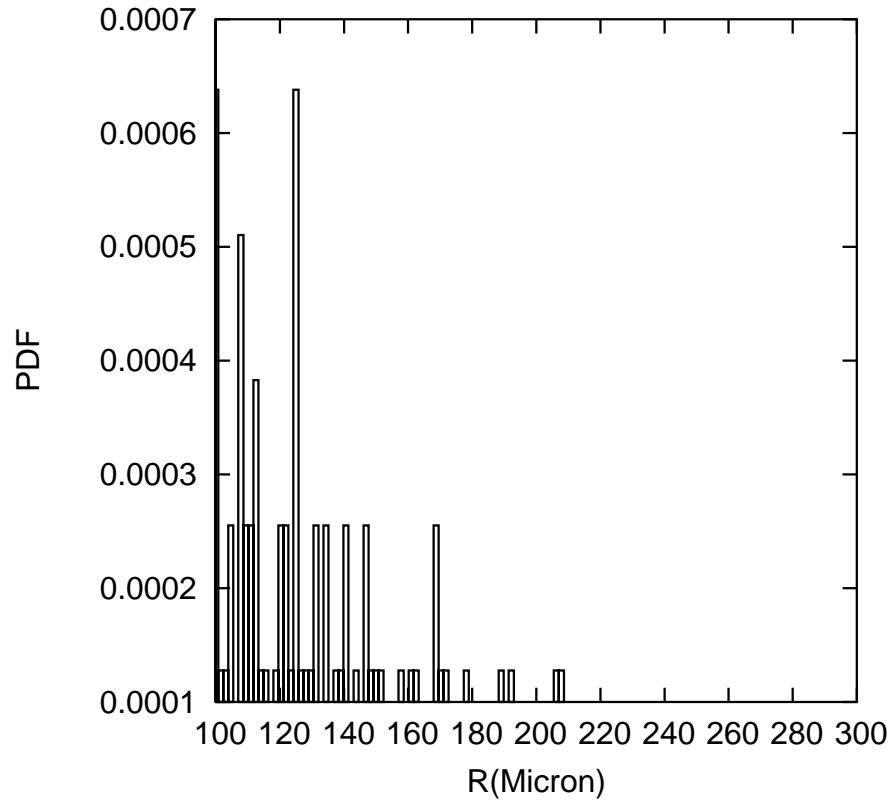


Figure 10: Measured bubble size distribution in the range $R > 100 \mu\text{m}$ for gas flow rates of 4 ml/min (top) and 8 ml/min; the water flow rate was 2.4 l/min.

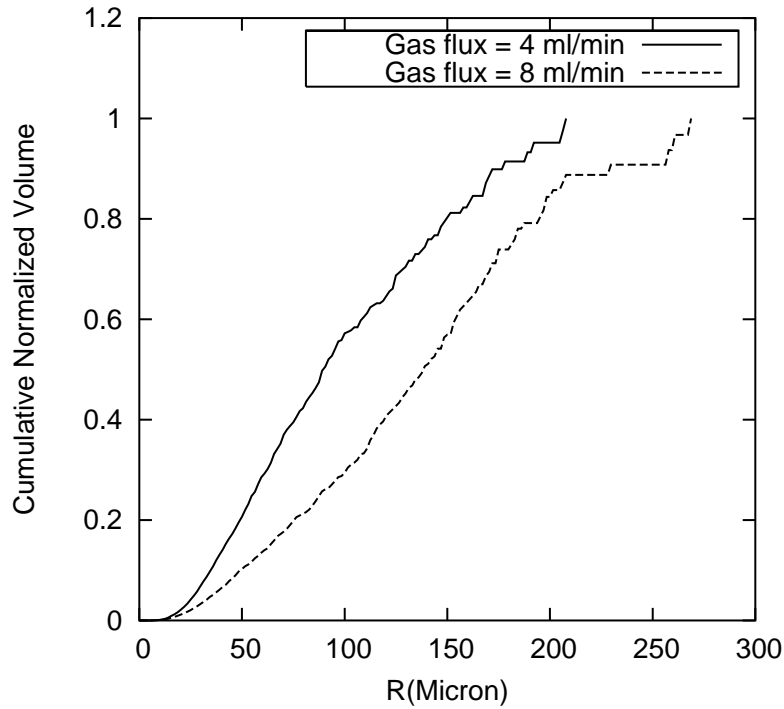


Figure 11: Normalized cumulative gas volume contained in bubbles with radius smaller than R as a function of the bubble radius R . The solid line is calculated from the data shown in the upper panels of Figures 9 and 10; the solid line, from the data shown in the lower panels.

might explain the paucity of bubbles larger than 50 to 100 μm found by Fujiwara et al. (2004) who used larger liquid flow rates, which would both increase the violence of collapse and inhibit coalescence due to the higher turbulence level. Higher liquid velocity, however, are of course energetically more expensive. Another possibility is that the larger gas volume fraction in the nozzle would reduce the violence of the collapse and, therefore, leave larger fragments to begin with. In view of the crucial importance of bubble size in the present application, this aspect of the results seems to warrant further study in the future.

These results show that, to some extent, control of the bubble size distribution can be obtained by adjusting the liquid and gas flux rates, although a precise way of achieving this goal must be the object of future research. While the matter cannot be resolved at this time, the present results confirm that the approach used in this study is an effective method to generate microbubbles.

Figure 11 shows the relative cumulative gas volume contained in bubbles smaller than R as a function of R according to the measured size distribution. In other words, the quantity shown is

$$\frac{1}{V_{gas,total}} \int_0^R \frac{4}{3}\pi R^3 PDF(R) dR \quad (2)$$

where $V_{gas,total}$ is the total amount of gas contained in the measured bubbles. The figure

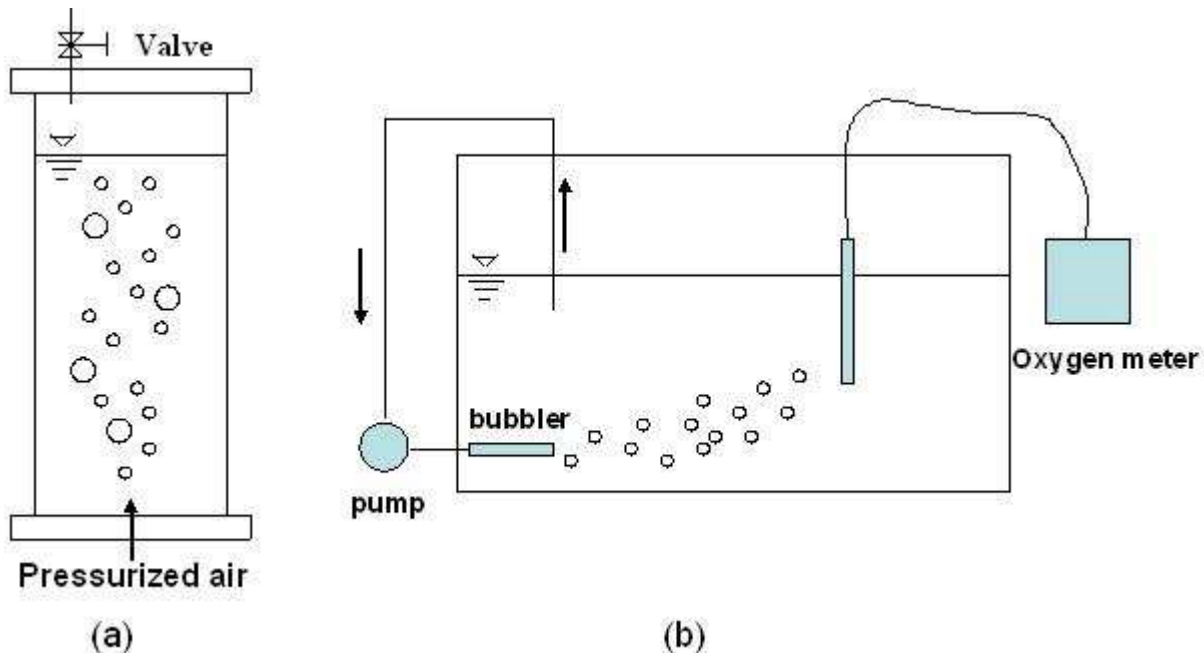


Figure 12: (a) Schematic of the PVC tank used to prepare the super-saturated gas solutions and to conduct some of the tests. (b) The glass tank in which the remaining tests were conducted.

shows that, for the 8 ml/min gas flow rate, a large fraction of the volume is contained in the larger bubbles. As a matter of fact, when it is remembered that the actual gas flow rate was twice as large in the case of the dashed curve, this figure shows that the absolute number of bubbles below $100 \mu\text{m}$ radius was probably comparable at the two gas flow rates.

4 Experimental set-up and procedure

In order to prepare water with the desired level of gas-super-saturation, we constructed a tank consisting of a PVC pipe with a diameter of 6" and a height of 6' (Figure 12a). Pressurized air was injected into the tank from the bottom. A valve installed on the lid of the tank was used to hold the internal pressure around 1.5 atm. After about 1-2 hours, a 130% saturation level could be reached. The water in the tank was then drained into a $48 \times 24 \times 30 \text{ cm}^3$ transparent glass tank (Figure 12b), to the bottom of which a bubbler was attached. An oxygen meter was used to monitor the water saturation level in the experiment. A pump was used to draw water from tank to run the bubbler in a closed-system fashion.

The oxygen concentration in the water was measured with a system¹ including a Po-

¹Quanta Water Quality Monitoring System, Hydrolab Corp., Austin, TX.

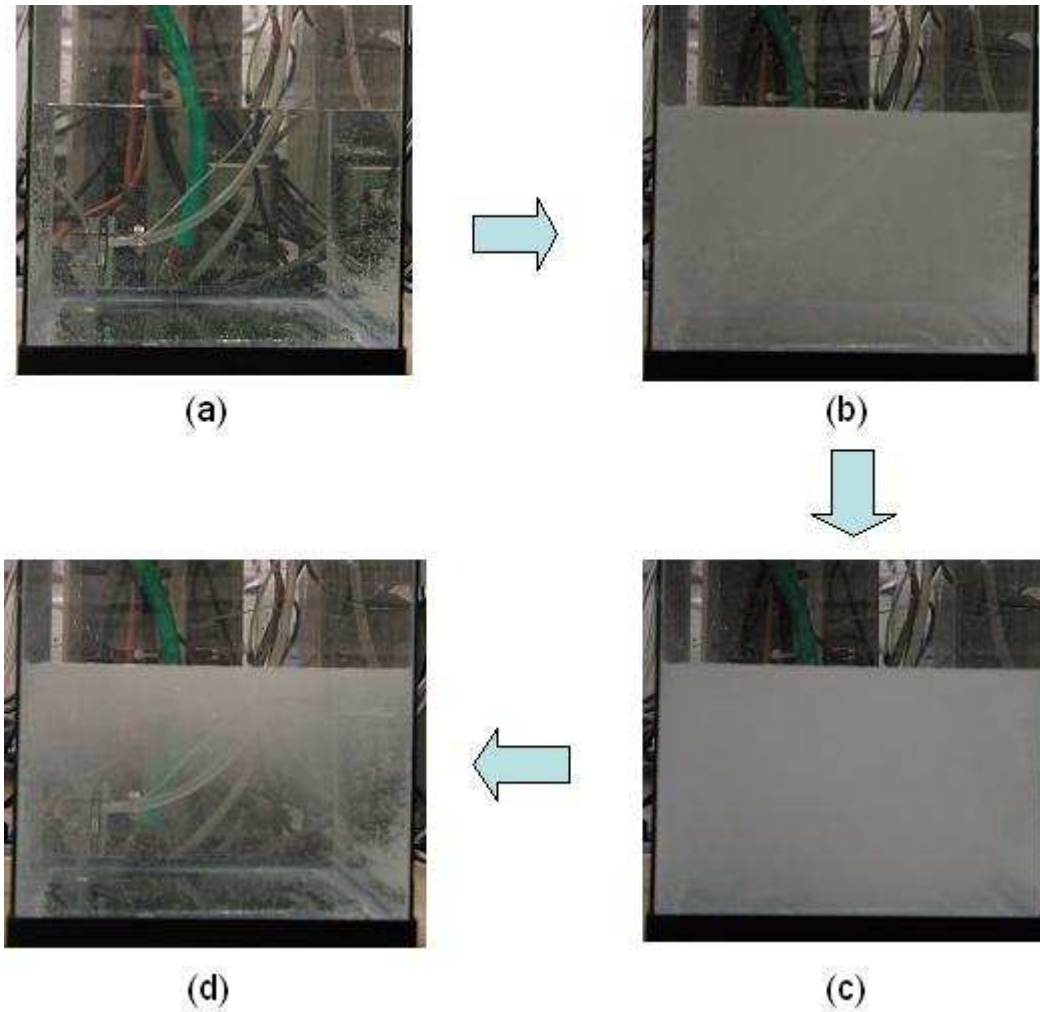


Figure 13: Typical sequence of events in the glass tank. The first picture shows the glass tank half-filled with the gas-super-saturated water before the bubbler is turned on. The bubbler is oriented toward the viewer and can be seen in the lower left corner. The second picture is taken just after the bubbler has run for 1 minute; the many small bubbles render the liquid opaque. After about 30 s, the opacity of the liquid increases further even though no more bubbles have been injected (third picture). One minute later the bubbles rise toward the water surface by buoyancy and the lower part of the tank starts to become clear (last picture).

larographic sensor with a diameter of about 15 mm. The reading usually stabilizes in a few tens of seconds. One problem that we encountered was due to the presence of a membrane on the tip of the sensor, to which bubbles might occasionally attach. For this reason we could not take accurate measurements in a bubbly flow continuously. Thus we adopted the

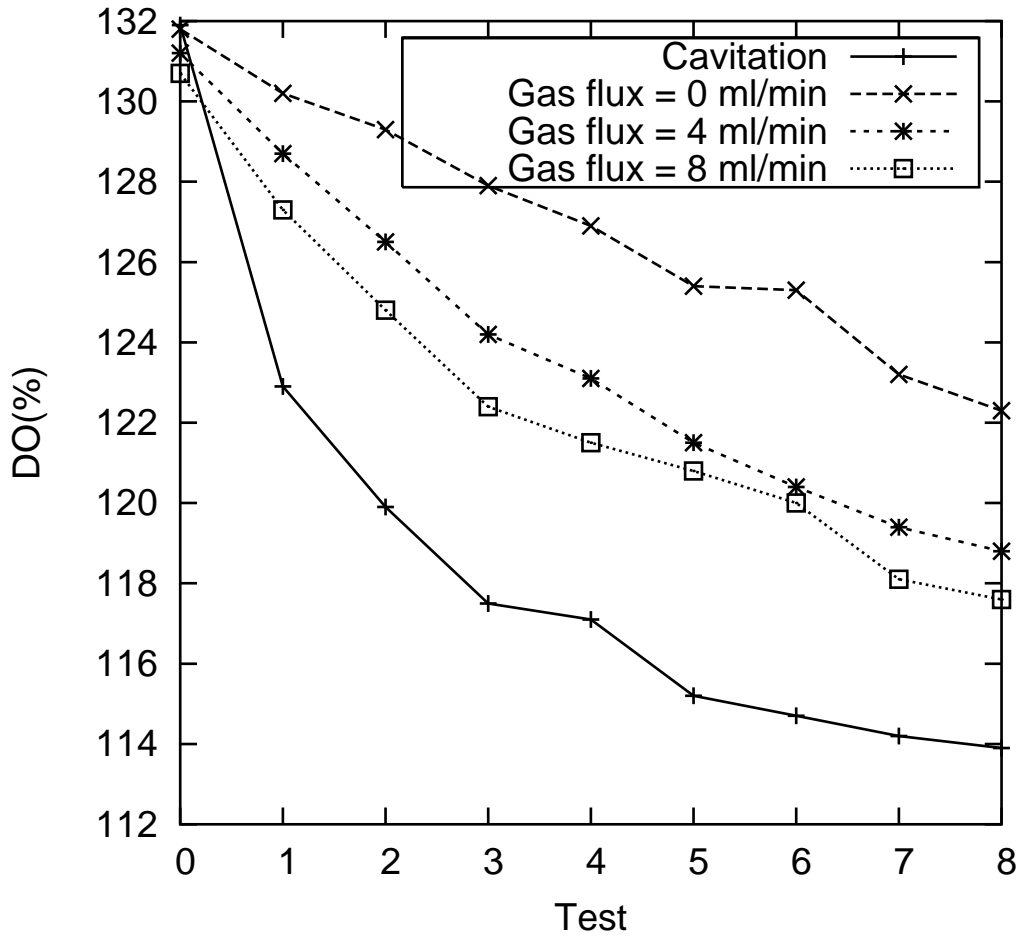


Figure 14: Dissolved oxygen concentration vs. time at 3 different gas flow rates, all for a water flow rate of 2.4 l/min, and with bubbles generated by cavitation at a water flow rate of 3.6 l/min.

following procedure. After filling the glass tank with water super-saturated to the desired level, the bubbler was run for 1 minute. After the time necessary for most bubbles to rise to the surface, a reading was taken of the oxygen concentration. Then the bubbler was run for another minute, and another reading taken. The same procedure was repeated eight times. In the figures that follow, the readings taken after 1, 2, ... minutes of bubbling are termed Test 1, Test 2, etc.

All tests were conducted with liquid temperatures between 20 and 25 °C.

5 Experimental results

Figure 13 shows a typical sequence of events. The first picture (Figure 13a) shows the glass tank half-filled with the gas-super-saturated water before the bubbler is turned on. The bubbler, located near the tank wall opposite the viewer, can be seen at the lower left; it is oriented toward the viewer.

The second picture is taken just after the bubbler has been run for 1 minute. At this point there are so many small bubbles in the tank that the liquid appears opaque (Figure 13b). After about 30 s, the opacity of the liquid has increased further and the color has become whiter even though no more bubbles have been injected (Figure 13c). This effect is due to the growth of bubbles by diffusion and is a clear indication of the degassing effect of the microbubbles. Due to buoyancy, the bubbles rise toward the water surface and, one minute later, the lower part of the tank begins to clear (Figure 13d).

Figure 14 presents some experimental results obtained in this way. The vertical axis is the percent dissolved oxygen with respect to the saturation level at the measured liquid temperature. The horizontal axis is the test number i.e., essentially, the number of minutes the bubbler was on as explained before in section 4.

The first feature to note is that the water flow by itself has an effect on the amount of dissolved oxygen even without the injection of any bubble (top-most line). This is due to the mixing induced by the water flow and the surface renewal process mentioned before in section 1. This effect is magnified in the present experiment by the relatively small size of the tank. The other three lines refer to runs in which the water jet contained gas bubbles due either to gas ingestion or cavitation.

In these cases, the dissolved oxygen level drops quickly during the first three minutes (i.e., shown as Tests 1, 2, and 3). The decline then slows down due to the falling dissolved oxygen level in the water. This development is due to the fact that the driving force for the gas to diffuse into the bubbles is determined by the difference between the gas concentration at the bubble surface, which is essentially at saturation, and the surrounding water.

It is at first sight surprising that the results for the 4 and 8 ml/min gas injection rates are very comparable. We believe that the reason for this unexpected small difference is the presence of larger bubbles in the 8 ml/min case as discussed in section 3. It was argued there that the absolute numbers of “small” bubbles may be comparable in the two cases, with the gas of the 8 ml/min case in excess of the 4 ml/min case being largely confined to large bubbles. As already noted, these large bubbles reduce the available gas/liquid interfacial area and are not very effective in removing the dissolved gas. This shortcoming is compounded by their short residence time in the liquid.

The importance of bubble size is strikingly illustrated by these results as well as those for the cavitating flow which indicate a much faster dissolved gas removal rate. As is evident from Figure 4, these bubbles are smaller than those deriving from the injection of gas.

Temperature (°C)	Mole Frn. $\times 10^4$	Ostwald Coeff. λ	K (moles/m ³ atm)	Diffusivity $\times 10^9$ (m ² /s)
0	0.3941	0.04902	2.190	
5	0.3458	0.04381	1.921	
10	0.3071	0.03960	1.706	1.54
15	0.2759	0.03618	1.533	
20	0.2505	0.03339	1.392	1.98
25	0.2298	0.03111	1.277	

Table 1: Physical properties for oxygen

Temperature (°C)	Mole Frn. $\times 10^4$	Ostwald Coeff. λ	K (moles/m ³ atm)	Diffusivity $\times 10^9$ (m ² /s)
0	0.1914	0.02381	1.063	
5	0.1695	0.02147	0.942	
10	0.1519	0.01959	0.844	1.29
15	0.1379	0.01808	0.766	
20	0.1265	0.01666	0.703	1.77
25	0.1173	0.01588	0.652	

Table 2: Physical properties for nitrogen

6 Bubble growth by diffusion

In order to explain the previous remark about the possibility for very small bubbles to impede rather than aid the degassing of a liquid, let us consider in some detail a bubble injected in a super-saturated liquid.

For the bubble to be in mechanical equilibrium with the surrounding liquid, the internal pressure P must equal the external pressure in the liquid P_L plus the contribution of surface tension:

$$P = P_L + \frac{2\gamma}{R} \quad (3)$$

where γ is the surface tension coefficient and R the bubble radius. If the bubble is at a depth H below the surface,

$$P_L = P_{atm} + \rho g H \quad (4)$$

where P_{atm} is the atmospheric pressure, ρ is the liquid density, and g the acceleration of gravity. The radius corresponding to this mechanical equilibrium condition is then

$$R = \frac{2\gamma}{P - P_L} \quad (5)$$

At the bubble surface, the concentration C_s of gas dissolved in the liquid satisfies Henry's law:

$$C_{s,O_2} = K_{O_2}(T)P_{O_2} \quad C_{s,N_2} = K_{N_2}(T)P_{N_2} \quad (6)$$

where the K 's are temperature-dependent quantities available from the literature (Ferrell & Himmelblau 1967; Wilhelm et al. 1977) and shown in Tables 1 and 2. If the surface concentration exceeds the ambient concentration C_∞ in the liquid, Henry's law will cause a gradient in the concentration which will promote a dissolution of the bubble. Conversely, if $C_s < C_\infty$, the gradient will drive gas to diffuse into the bubble and the bubble will grow. An equilibrium is possible only if $C_s = C_\infty$.

Tables 1 and 2 show a few values of the solubility and diffusivity of oxygen and nitrogen as a function of temperature. The solubility is expressed in two different ways. The Ostwald coefficient λ is defined as the ratio of the volume of saturating gas to the volume of pure solvent at the temperature and pressure of the experiment. The mole fraction N is the number of gas moles dissolved in a mole of liquid at 1 atm at each temperature. From the perfect gas law, one mole of gas at 0 °C and 1 atm occupies a volume of 22.4 l, while one mole of water occupies a volume of 18 cm³ or 0.018 l. Thus

$$\lambda = 1.24 \times 10^3 \times N \frac{273.15 + T}{273.15} \quad (T \text{ in } ^\circ\text{C}) \quad (7)$$

It is important to note that the solubility of oxygen is about twice as large as that of nitrogen.

While, in addition to nitrogen and oxygen, the bubbles will contain argon, carbon dioxide, water vapor, and other gases, we will only consider nitrogen and oxygen which typically make up about 97% of the gaseous content of each bubble.² With this approximation, the internal bubble pressure is given by the sum of the partial pressures:

$$P = P_{O_2} + P_{N_2} \quad (8)$$

But, in an equilibrium situation, the partial pressures are given by (6) with $C_s = C_\infty$:

$$P_{O_2} = \frac{C_{\infty,O_2}}{K_{O_2}} \quad P_{N_2} = \frac{C_{\infty,N_2}}{K_{N_2}} \quad (9)$$

By combining the previous results, we find the radius of a bubble in both mechanical and diffusive equilibrium in a liquid:

$$R = \frac{2\gamma}{(C_{\infty,O_2}/K_{O_2}) + (C_{\infty,N_2}/K_{N_2}) - P_{atm} - \rho gH} \quad (10)$$

The equilibrium described by this relation is however unstable as the following argument shows. Suppose that the bubble radius decreases by a slight amount below the value given

²Normal air consists of approximately 78% nitrogen, 21% oxygen, 1% argon, and 0.03% carbon dioxide. The partial pressure of water vapor at 20 °C is about 2.3 kPa, i.e., 2.3% of one atmosphere.

by (10). Then Eq. (3) shows that the combined effect of the liquid pressure and surface tension will overpower the internal pressure. As a result of this situation, the bubble will shrink, with a consequent increase in its internal pressure. From Henry’s law, this pressure increase raises the concentration of dissolved gases at the bubble surface. This process sets up concentration gradients in the liquid which will promote a dissolution of the bubble. Conversely, as a consequence of a small radius increase, the bubble internal pressure will be larger than the right-hand side of (3). The bubble will then try to expand, which lowers its internal pressure, and causes concentration gradients which will tend gas to diffuse toward the bubble, which will then grow further.

While therefore the equilibrium described by (10) is unstable, this argument shows that the introduction, in a super-saturated liquid, at a depth H of bubbles smaller than the value given by (10) will be counter-productive as the bubbles will actually dissolve and increase the concentration of dissolved gas.

It is important to note that the effect of surface tension can be very large for small bubbles. For illustration purposes, let us consider only one gas and assume $P_L = P_{atm}$. Then, for a bubble with a radius $10 \mu\text{m}$, the surface tension term amounts to about 14% of the pressure in the liquid. Thus, if the concentration of dissolved gas is less than 114%, the bubble will dissolve rather than grow.

7 Mathematical model and numerical simulation

In order to better understand the experimental results – and in particular the effect of bubble size on the gas diffusion – it is useful to have recourse to a simple mathematical model. Furthermore, since we did not have a nitrogen concentration meter, we could not monitor the dissolved concentration of this gas in spite of its demonstrated importance in the fish kills due to water super-saturation. Thus, the numerical model will also be useful in providing insight on the evolution of the nitrogen concentration as well.

We suppose that bubbles are uniformly injected at the tank bottom $z = 0$. We neglect the liquid flow and simply allow the bubbles to rise to the surface with their terminal rising velocity. It is assumed that, at each level z , the bubbles are immersed in a liquid having the average concentration at that level. Thus, dissolved gas gradients in the liquid are neglected. With these assumptions, we can build a simple one-dimensional model as follows.

Since bubbles with different sizes rise at different speeds and are able to absorb different amounts of dissolved gases, it is important to track their evolution in dependence of their initial size R_0 . If $n(z, t, R_0)$ is the number density of bubbles with an initial size R_0 at level z and time t , conservation of the bubble number is expressed by

$$\frac{\partial n}{\partial t} + \frac{\partial}{\partial z}(nu_b) = 0 \tag{11}$$

where $u_b(R)$ is the radius-dependent rise velocity of the bubbles. We estimate this quantity by using a standard correlation for the drag coefficient for spheres (see e.g. Clift, Grace &

Weber 1978), namely

$$C_D = \frac{24}{Re} (1 + 0.15Re^{0.687}) \quad (12)$$

Here

$$C_D = \frac{\frac{4}{3}\pi R^3 \rho g}{\frac{1}{2}\pi R^2 \rho u_b^2} = \frac{8Rg}{3u_b^2} \quad (13)$$

where $R(t)$ is the instantaneous bubble radius and g the acceleration of gravity. The Reynolds number Re is defined by

$$Re = \frac{2Ru_b}{\nu} \quad (14)$$

where ν is the liquid kinematic viscosity. Equation (12) is applicable from very small Reynolds numbers to about $Re = 1000$ and is therefore more than sufficient to cover our experimental range where Reynolds numbers are of the order of 10 or smaller, with perhaps a few large bubbles rising with $Re \sim 50$ or so. In these equations we use the instantaneous radius, which is permissible due to its slow rate of variation. The correlation (12) was originally developed for solid spheres, but the bubbles of present concern closely approximate these conditions because they are small enough to be very nearly spherical. Furthermore, since bubbles are almost invariably contaminated with surface active substances, their surface will essentially behave as rigid.

The moles of oxygen, m_{1b,O_2} , and nitrogen, m_{1b,N_2} , in each bubble satisfy evolution equations of the form

$$\frac{\partial m_{1b,O_2}}{\partial t} + u_b \frac{\partial m_{1b,O_2}}{\partial z} = S_{1b} \dot{m}_{1b,O_2} \quad (15)$$

$$\frac{\partial m_{1b,N_2}}{\partial t} + u_b \frac{\partial m_{1b,N_2}}{\partial z} = S_{1b} \dot{m}_{1b,N_2} \quad (16)$$

Here $S_{1b} = 4\pi R^2$ is the surface area of the bubble and \dot{m}_{1b,O_2} and \dot{m}_{1b,N_2} are the molar fluxes at the bubble surface. These relations state that the amount of gas in each bubble is convected upward with velocity u_b and is augmented by an amount $S_{1b} \dot{m}_{1b} \Delta t$ during each elementary time interval Δt . It may be noted that adding (11) multiplied by m_{1b} to either (15) or (16) multiplied by n gives

$$\frac{\partial}{\partial t}(nm_{1b}) + \frac{\partial}{\partial z}(nm_{1b}u_b) = S_{1b} \dot{m}_{1b} n \quad (17)$$

valid for either gas. Upon integration of this equation between a level z_1 and a level z_2 we have

$$\frac{d}{dt} \int_{z_1}^{z_2} nm_{1b} dz = [nm_{1b}u_b]_{z_1} - [nm_{1b}u_b]_{z_2} + \int_{z_1}^{z_2} S_{1b} \dot{m}_{1b} n dz \quad (18)$$

which simply states that the rate of change of the amount of gas contained in bubbles of a certain initial radius residing in the liquid layer $z_1 \leq z \leq z_2$ receives positive contributions from the influx from the lower surface at z_1 and the gas diffusing into the bubbles inside the layer, and a negative contribution from the bubbles leaving the upper surface at z_2 .

The mass transfer rate \dot{m}_{1b} is proportional to the difference between the concentration at the bubble surface, C_s , and in the liquid, C_∞ , and can be represented as

$$\dot{m}_{1b} = h_m (C_\infty - C_s) \quad (19)$$

where h_m is the mass transfer coefficient and C_{s,O_2} , C_{s,N_2} are expressed in terms of the respective partial pressures in the bubble by (6). The subscript ∞ signifies that C_∞ is the ‘‘ambient’’ gas concentration seen by each bubble which we identify with the mean concentration in the liquid at the level of the bubble.

For the mass transfer coefficient, we use an experimental relation developed by Takemura & Yabe (1998) to estimate the Sherwood number Sh

$$Sh = \frac{2Rh_m}{D} \quad (20)$$

in which D is the gas diffusivity in the liquid. This correlation has the form

$$Sh = \frac{2}{\sqrt{\pi}} \left[1 - \frac{2}{3} \frac{1}{(1 + 0.09Re^{2/3})^{3/4}} \right]^{\frac{1}{2}} (2.5 + Pe_D^{1/2}) \quad (21)$$

where

$$Pe_D = \frac{2Ru_b}{D} \quad (22)$$

is the Péclet number for diffusion. This relation is valid for $Re < 100$, $Pe_D > 1$ which, for the present case, corresponds to $Re \geq 10^{-3}$, approximately.

At each level z in the liquid we write an equation for the evolution of the average dissolved gas concentrations C_{∞,O_2} and C_{∞,N_2} in the form

$$\frac{\partial C_{\infty,O_2}}{\partial t} = - \int n S_{1b} \dot{m}_{1b,O_2} dR_0 \quad (23)$$

$$\frac{\partial C_{\infty,N_2}}{\partial t} = - \int n S_{1b} \dot{m}_{1b,N_2} dR_0 \quad (24)$$

where the integration is over the size range of the bubbles introduced at the bottom of the tank.

A knowledge of the number of moles in the bubble enables us to calculate the bubble radius from the perfect gas law:

$$\frac{4}{3}\pi R^3 P = (m_{1b,O_2} + m_{1b,N_2}) \mathcal{R}T \quad (25)$$

Since the bubble is essentially in mechanical equilibrium, for P we take

$$P = P_{atm} + \rho g(h - z) + \frac{2\gamma}{R} \quad (26)$$

where z is measured from the point of injection of the bubbles at a depth h below the free surface. For perfect gases, the partial pressures are in the same ratio as the mole fractions:

$$\frac{P_{O_2}}{P_{N_2}} = \frac{m_{1b,O_2}}{m_{1b,N_2}} \quad (27)$$

so that, for example,

$$P_{O_2} = \frac{m_{1b,O_2}}{m_{1b,O_2} + m_{1b,N_2}} \left[P_{atm} + \rho g(h - z) + \frac{2\sigma}{R} \right] \quad (28)$$

The system of equations presented here is closed and permits to calculate the evolution of the dissolved oxygen concentration in the liquid once the initial bubble size distribution has been prescribed. For this quantity, we make several choices so as to consider different situations as described below.

8 Numerical method

The previous equations were discretized by simple first-order methods in space and time. For example, Eq. (11) was discretized as

$$\frac{n_i^{k+1} - n_i^k}{\Delta t} + \frac{n_i^k (u_b)_i^k - n_{i-1}^k (u_b)_{i-1}^k}{\Delta z} = 0 \quad (29)$$

where $n_i^k = n(i\Delta z, k\Delta t)$ for $i = 1, 2, \dots, N_z$. The spacing of the spatial nodes was between 3 and 5 mm, and the time step around 1 ms.

The integrations in (23) were effected as

$$\frac{(C_{\infty,O_2})_i^{k+1} - (C_{\infty,O_2})_i^k}{\Delta t} \simeq - \sum_{J=1}^{N_{R_0}} n_i^k(R_{0,J}) (S_{1b})_i^k(R_{0,J}) (\dot{m}_{1b,O_2})_i^k(R_{0,J}) \Delta R_0 \quad (30)$$

where N_{R_0} is the number of subdivisions of the range for the radius integration, typically of the order of 100.

9 Numerical results

Figure 15 is a comparison of numerical results for the average dissolved oxygen concentration with the experimental ones shown in Figure 14 for 4 ml/min and 8 ml/min gas flow rates. The corresponding gas fluxes, obtained by dividing by the cross-sectional area of the glass tank, are $3.47 \times 10^{-3} \text{ cm}^3/(\text{cm}^2 \text{ min})$ and $6.94 \times 10^{-3} \text{ cm}^3/(\text{cm}^2 \text{ min})$ respectively. For the calculations we used the measured bubble size distribution rather than the log-normal fit. The match is very good.

We also carried out experiments and a parallel numerical simulation in the PVC pipe, where the water height was 1.15 m. We used the same bubbler as for the glass tank and

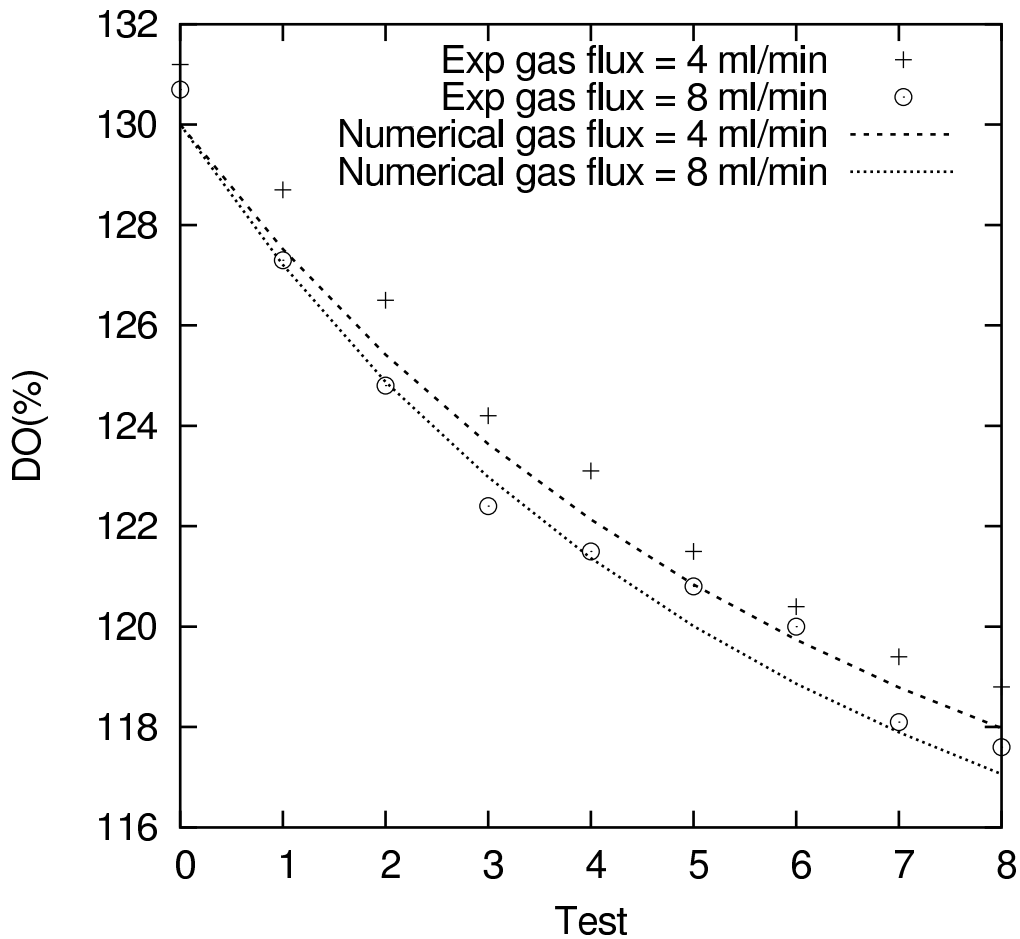


Figure 15: Comparison of numerical results for the average dissolved oxygen concentration with the experimental ones shown in Figure 14 for 4 ml/min and 8 ml/min gas flow rates. The measured bubble size distribution was used in the numerical calculation.

therefore, since the cross sectional area of this pipe was much smaller than that of the glass tank, the bubble number density was considerably greater. For a gas flow rate of 4 ml/min, in this tank the gas flux is $21.9 \times 10^{-3} \text{ cm}^3 / (\text{cm}^2 \text{ min})$.

The experimental results were collected at three different depths. Since the liquid is well mixed, the dissolved oxygen concentrations are almost the same at different depths in each test. However, the solubility increases as water depth increases due to the effect of hydrostatic pressure. Over a depth of 1 m, the effect is about a 10% difference between the top and bottom of the pipe, which is reflected in the data shown in Figure 16. This is the reason why the relative saturation of dissolved oxygen in the experiment is larger at the water surface, and smaller at the bottom. Because of the larger bubble number density there is a large drop of the dissolved oxygen concentration already after 1 minute of bubbling (Test 1). The change of dissolved oxygen concentration is quite small in the subsequent tests.

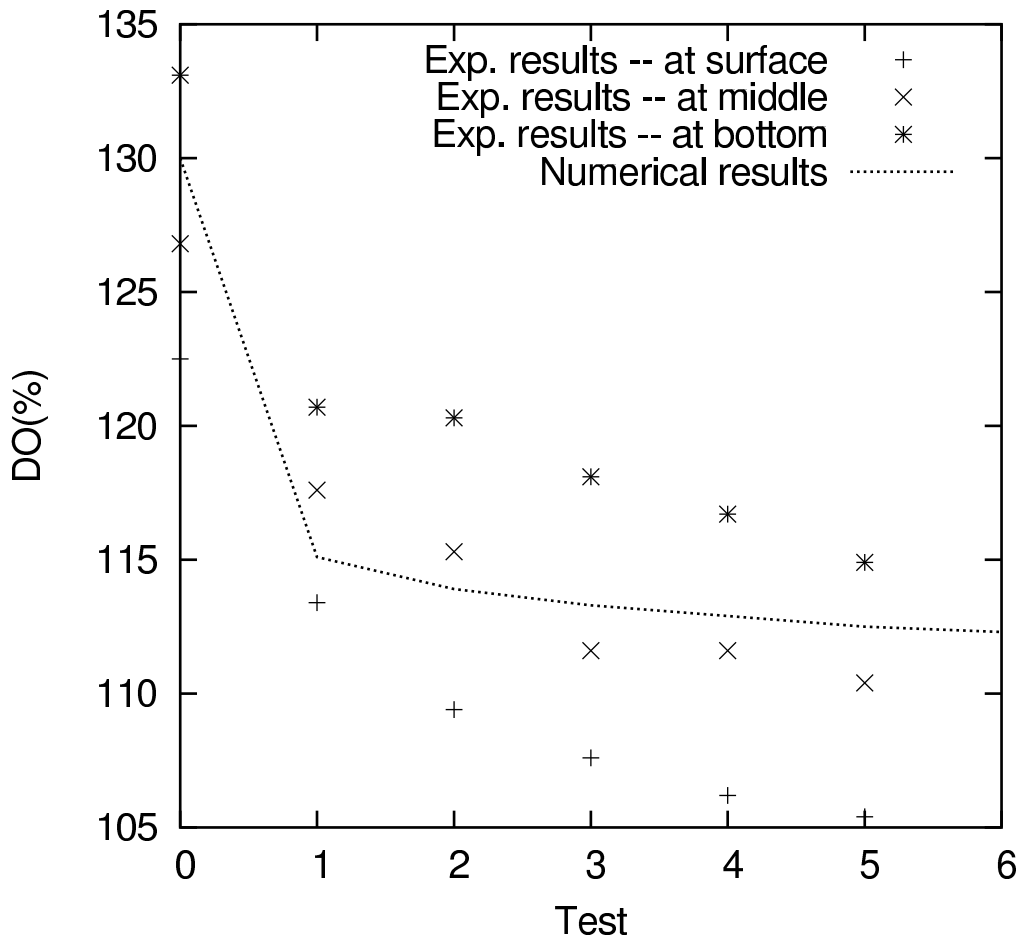


Figure 16: The symbols are concentration data taken at three depths in the PVC pipe. Because of the large bubble number density the dissolved oxygen concentration is strongly reduced already after 1 minute of bubbling (Test 1). The line shows the numerical results averaged over the depth of the pipe. The gas flux is 4 ml/min.

The line shows the numerical results averaged over the depth of the pipe. The reason to present results in this way is that the bubbling induces a convective mixing of the liquid which is not reflected in the model. This effect is stronger in this PVC pipe than in the glass tank in view of the smaller cross sectional area. The figure shows that the theoretical line represents a good average of the measured data.

These tests indicate that the model is capable of giving a fair representation of the process under study. It is therefore interesting to carry out further simulations to explore additional aspects of the process.

In the figures that follow, the results are presented so as to mimic the procedure by which the concentration levels were measured in the experiment. To recapitulate: the line labelled Test 0 shows the initial profile. The simulation is started with bubbles injected uniformly from the tank bottom for 1 minute, and stopped when all the bubbles have

risen to the water surface. The result is the line labelled Test 1. The liquid concentrations established after this first one minute of bubbling are used as initial condition for the second minute, and so on.

Figures 17 show the effect of bubble size on the reduction of dissolved oxygen (top) and nitrogen. Here we show the time development of the dissolved gas concentration for different bubble radii. The gas flux is $3.47 \times 10^{-3} \text{ cm}^3/(\text{cm}^2 \text{ min})$ for all cases which corresponds, given the cross-sectional area of our glass tank, to 4 ml/min of gas. For the 10 and 20 μm -radius bubbles there is a precipitous drop already during the first minute of bubbling, and subsequent bubbling has little effect. As the bubble radius is increased to 50 and 100 μm , there is a strong decline in the degassing efficiency. These results agree with the superior performance of the cavitating nozzle shown in Figure 14, which produces smaller bubbles as observed before in connection with Figure 4.

A more detailed view of these results is shown in Figure 18 which shows the dissolved gas concentration as a function of depth for bubbles with an initial radius of 50 μm . The air flux is 34.7 ml/(min \times m²), corresponding to about 110 bubbles/(cm² s). The initial super-saturation (vertical line) is 130% for both oxygen and nitrogen. Note that this is referenced to the local hydrostatic pressure and, therefore, the *mass density* of the dissolved gas increases by about 10% from the surface to the bottom of the tank. The figure shows that the dissolved oxygen concentration has a relative maximum near the bottom of the tank. To understand this feature, we note that the bubbles injected are air bubbles, and therefore contain about 20% oxygen and 80% nitrogen. The partial pressure of the oxygen, therefore, is very low and the bubbles quickly absorb this gas. As a consequence of the rapidly rising oxygen partial pressure, the potential for uptaking more oxygen quickly decreases and so does the effectiveness for oxygen removal. As the bubble rises further, however, it expands due to the combined effect of the gas influx and falling hydrostatic pressure. This increases the bubble surface area and, with it, the uptake of dissolved oxygen. The nitrogen concentration depth dependence instead is monotonic because the initial nitrogen partial pressure in the bubble is much higher and, therefore, the nitrogen mass flux much smaller.

The concentration at higher levels and, in particular, at the top of the tank ends up being less for nitrogen than for oxygen. To explain this feature, we note that, if we assume for simplicity $D_{O_2} \simeq D_{N_2}$ (see Tables 1 and 2), the ratio of the molar fluxes is

$$\frac{\dot{m}_{O_2,1b}}{\dot{m}_{N_2,1b}} \simeq \frac{C_{O_2,\infty} - C_{O_2,s}}{C_{N_2,\infty} - C_{N_2,s}} \quad (31)$$

The liquid was prepared in such a way as to be in equilibrium with air at 1.3 atm, with the two gases having mole fractions of approximately 1/5 for oxygen and 4/5 for nitrogen. In view of the fact that the solubility of oxygen is about twice as large as that of nitrogen, therefore, $C_{O_2,\infty} \simeq 2 \times (1/4) C_{N_2,\infty} \simeq (1/2) C_{N_2,\infty}$. With these estimates, Eq. (31) may be rewritten as

$$\frac{\dot{m}_{O_2,1b}}{\dot{m}_{N_2,1b}} \simeq \frac{1}{2} \frac{1 - 2(C_{O_2,s}/C_{N_2,s})(C_{N_2,s}/C_{N_2,\infty})}{1 - C_{N_2,s}/C_{N_2,\infty}} \quad (32)$$

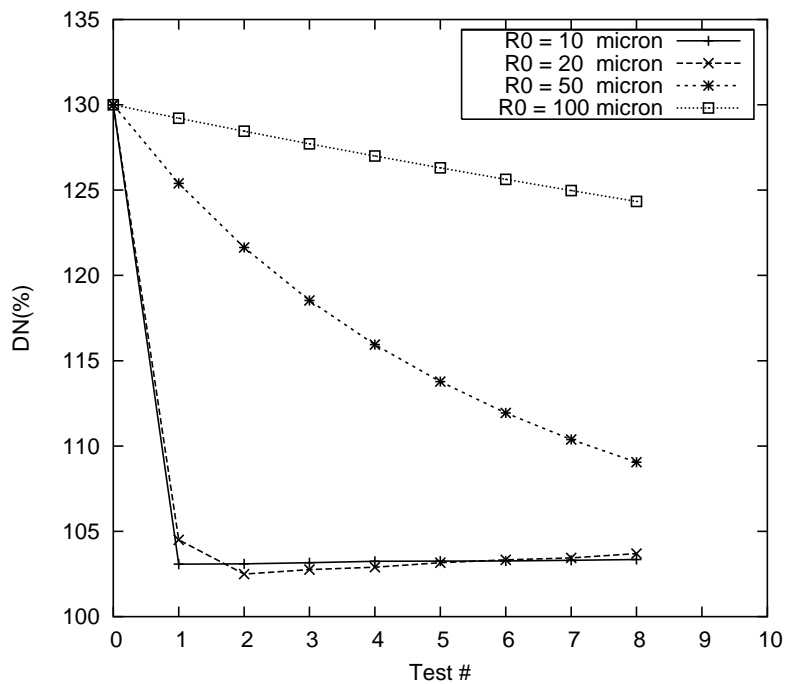
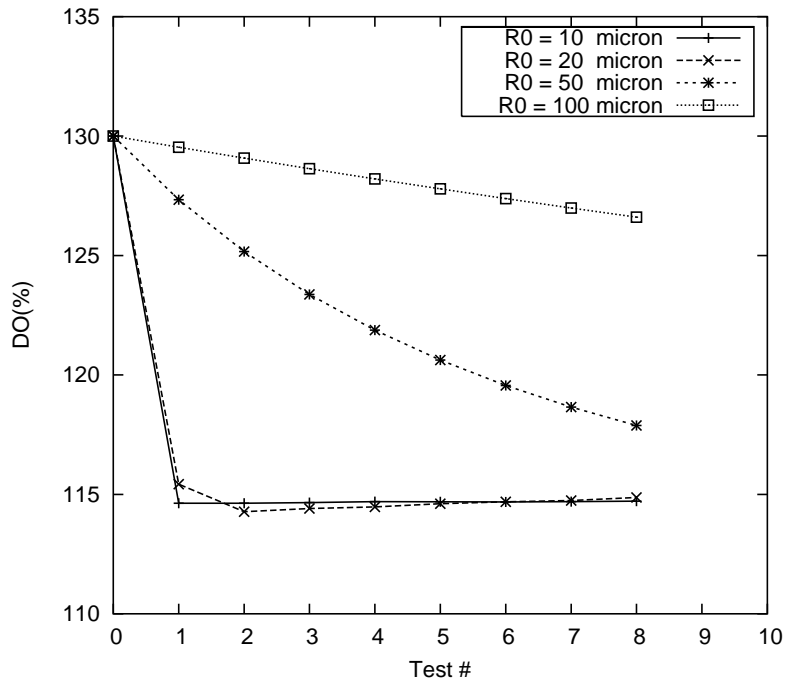


Figure 17: Calculated dissolved oxygen (top) and nitrogen concentration vs. time for 4 different bubble radii. The initial dissolved concentration for both oxygen and nitrogen was the equilibrium concentration with air at 1.3 atm and, therefore, was 130% of saturation. The gas flux is the equivalent of 4 ml/min in our glass tank.

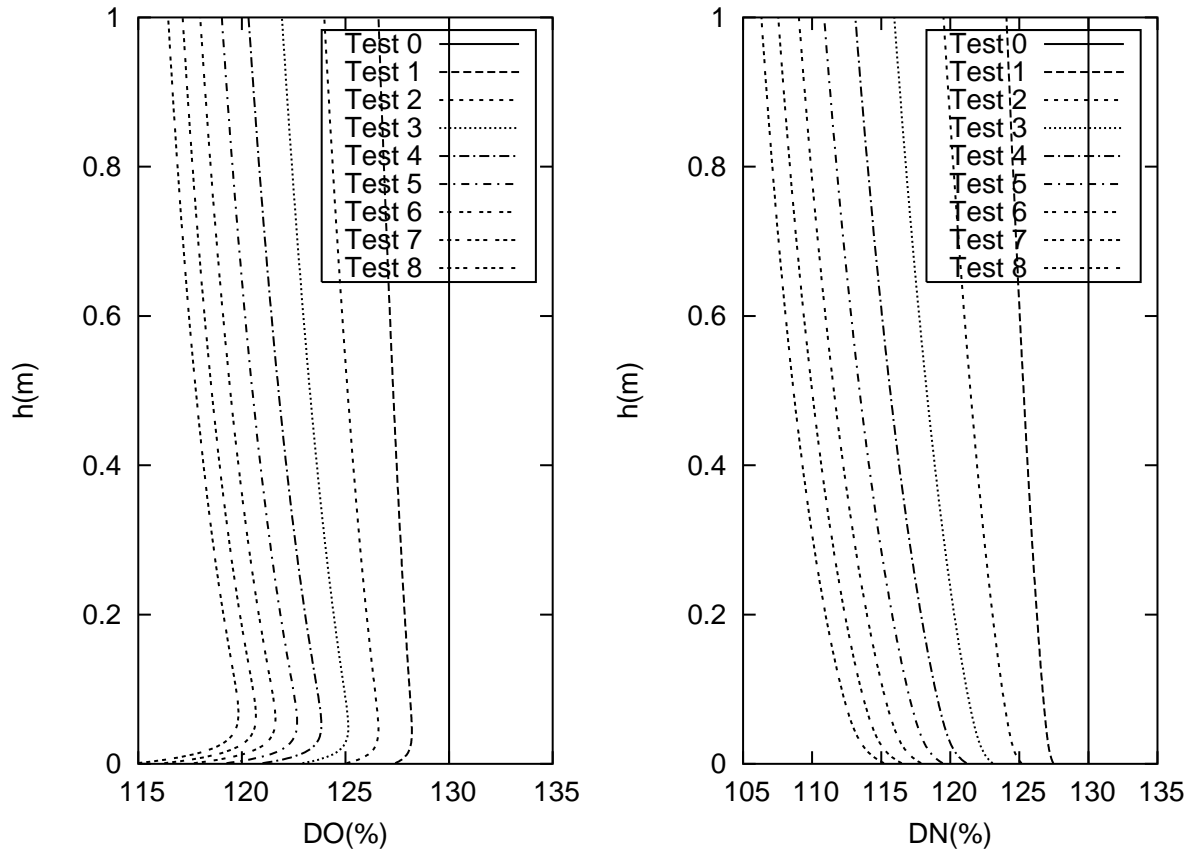


Figure 18: Dissolved gas concentration as a function of depth for bubbles with an initial radius of $50 \mu\text{m}$; the initial super-saturation (vertical line) is 130% for both oxygen and nitrogen.

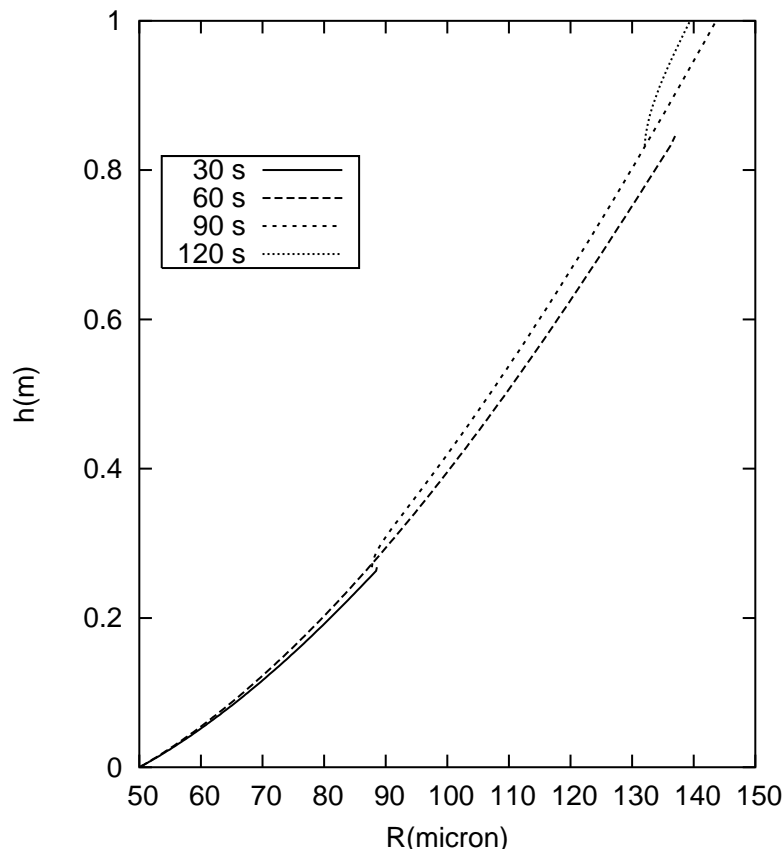


Figure 19: Calculated bubble radius distribution over the depth of the tank at various times after the beginning of bubbling for the case of Figure 18. Bubbling lasts for the first 60 s only.

If we use $\dot{m}_{O_2,1b}/\dot{m}_{N_2,1b} \simeq 1/2$ to estimate the ratio of the mass additions to the gases in the bubble, we have

$$\frac{C_{O_2,s}}{C_{N_2,s}} = \frac{m_{1b,O_2}(t)}{m_{1b,N_2}(t)} \simeq \frac{m_{1b,O_2}(0) + \Delta m_{1b,O_2}}{m_{1b,N_2}(0) + 2\Delta m_{1b,N_2}(0)} \quad (33)$$

where we have used the fact that the concentration is proportional to the partial pressure which, in its turn, is proportional to the mole fraction. It is easy to show that, provided $m_{1b,O_2}(0)/m_{1b,N_2}(0) < 1/2$ the fraction is an increasing function of $\Delta m_{1b,O_2}$. Since, initially, the ratio $m_{1b,O_2}(0)/m_{1b,N_2}(0)$ is approximately $1/4$, the condition is satisfied, which implies that the moles of oxygen increase with respect to those of nitrogen even though the mass flux of the latter into the bubble is about twice as large as that of the oxygen. The end result is that the bubbles are more effective at removing nitrogen than oxygen. Particularly in view of the strong influence of dissolved nitrogen in the fish kills due to super-saturation, it would be of great interest to substantiate this theoretical prediction with actual data. Unfortunately, the lack of a nitrogen meter prevented us from following up on this point.

Figure 19 shows, for the same initial bubble radius of $50 \mu\text{m}$, the bubble radius distribution over the depth of the tank 30 s after the beginning of bubble injection, at the end of the bubble injection period (60 s), 30 s later (90 s), and 60 s later (120 s), i.e., a full minute after the end of the injection. After 30 s from the beginning of bubble injection,

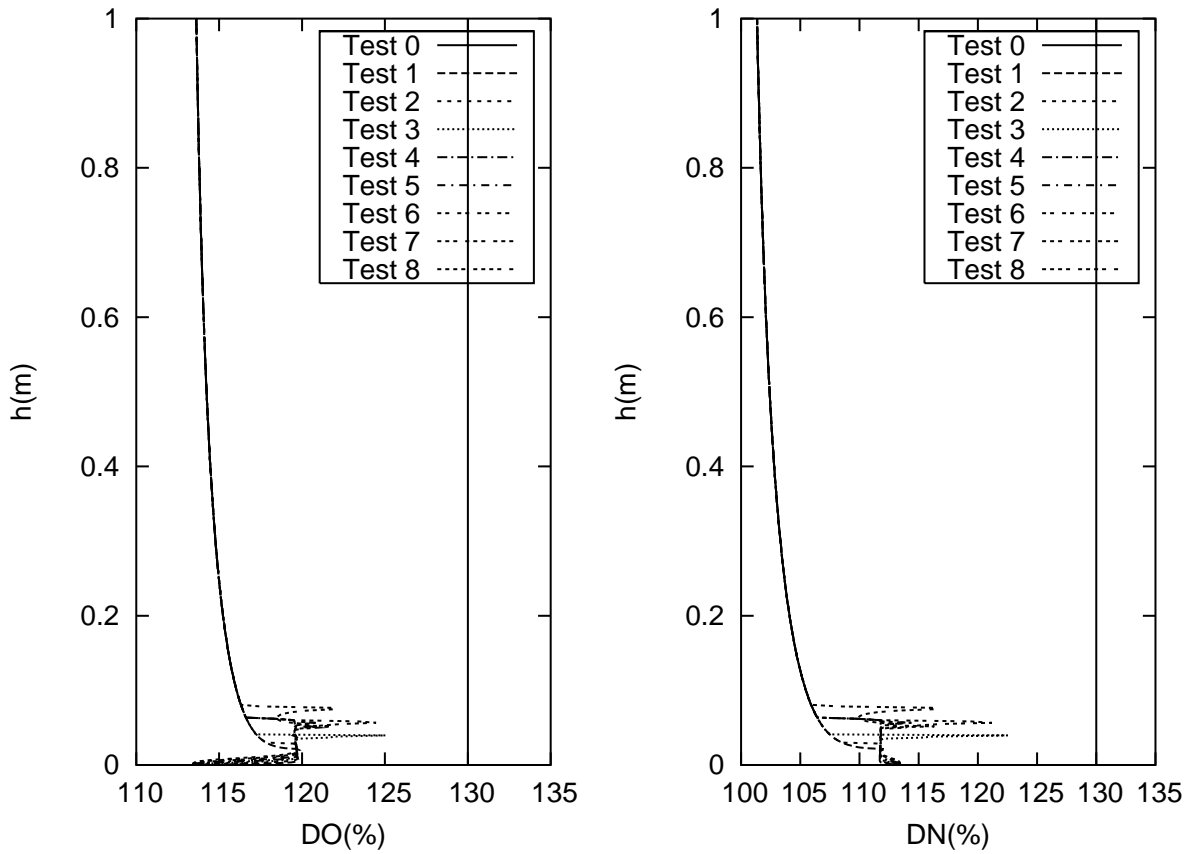


Figure 20: Dissolved gas concentration as a function of depth for bubbles with an initial radius of $10 \mu\text{m}$; the initial super-saturation (vertical line) is 130% for both oxygen and nitrogen. After two minutes of bubbling (Tests 2, 3, etc.) the liquid is so depleted of gas that the bubbles actually dissolve and do not reach the surface.

the bubbles have only risen to a depth of about 25 cm. The bubbles injected after this period find a slightly depleted gas concentration and therefore grow less. The bubbles that were injected between 0 and 30 s, in the meantime, have risen up to a level of about 85 cm and have correspondingly grown substantially to a maximum radius of about $140 \mu\text{m}$. Bubbling stops at 60 s and, therefore, there are no bubbles in the lower region of the tank for the lines corresponding to 90 and 120 s. These lines begin in the middle of the tank, which is where the last injected bubbles are to be found at these times.

Similar results for bubbles with an initial radius of $10 \mu\text{m}$ are shown in Figure 20. The air flux is the same as before, $34.7 \text{ ml}/(\text{min} \times \text{m}^2)$, but now the bubble injection rate is much greater, about $13,750 \text{ bubbles}/(\text{cm}^2 \text{ s})$.

After 1 minute the concentration of both gases has fallen dramatically reaching a level of about 113% for oxygen and 102% for nitrogen at the top of the tank. Subsequent bubbles encounter a gas-depleted liquid and, due to the effect of surface tension, actually lose their gas to the surroundings and dissolve completely never reaching the surface. This phenomenon is responsible for the increased dissolved gas concentration at later times near the bottom.

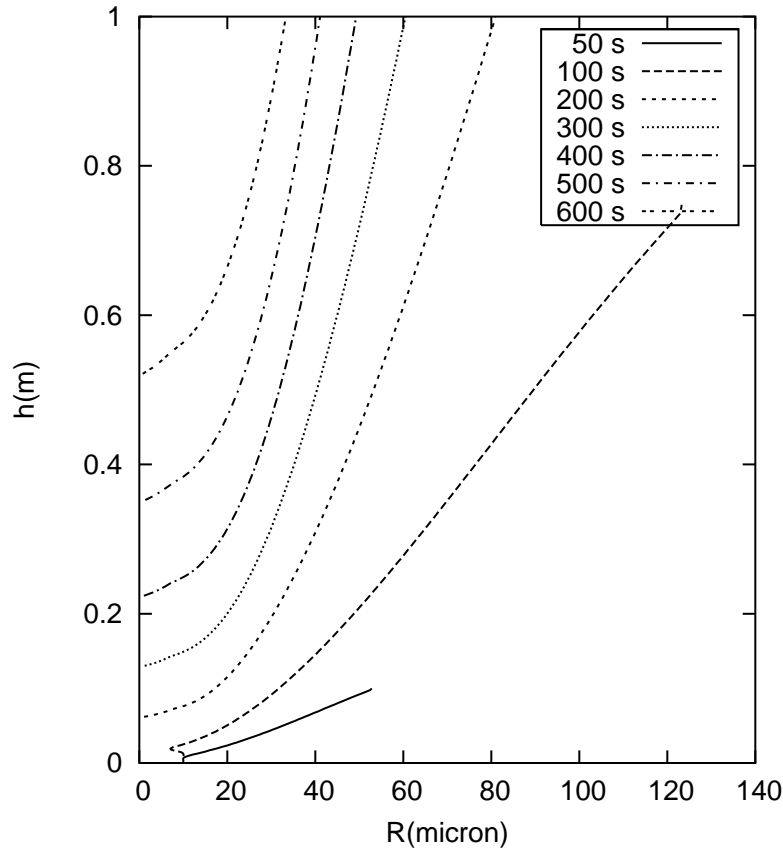


Figure 21: Calculated bubble radius distribution over the depth of the tank at various times after the beginning of bubbling for the case of Figure 20. Bubbling lasts for the first 60 s only.

The bubble size distribution for this case is shown in Figure 21. The appearance of this figure is strikingly different from the earlier picture in Figure 19 because, in this case, all the bubbles injected after the first 60 s-injection period dissolve. Thus, at 200 s and later times, there are no bubbles below a certain level. Above this level, the only bubbles to be found are those injected so early that they could grow or, at least, not dissolve.

Figure 22 shows the dissolved oxygen concentration averaged over the height of the tank vs. time when the number of bubbles injected per unit area and time is kept fixed at 110 bubbles $/(cm^2 s)$, while the initial bubble radius is varied from 10 to 100 μm . The larger surface area of the larger bubbles causes a more rapid gas removal, but there does not seem to be a great advantage in going from 10 to 20 or even 50 μm radii. The reason is that such small bubbles grow so rapidly that their initial size is not very relevant. This result poses a delicate optimization problem as, on the one hand, generating very small bubbles is not easy but, on the other hand, the smaller the gas flux the less energy is necessary to inject it into the liquid.

10 Conclusions

The objective of this study was to investigate whether the novel method to produce large numbers of small bubbles described in section 2 is an effective and promising approach to the degassing of super-saturated water bodies.

The scale of the experiments that we conducted was suitable for the laboratory and, therefore, much smaller than any future realistic application of this technique. Nevertheless, we found that indeed large numbers of microbubbles could be easily produced in this way. Furthermore, bubbles of the size that we could generate in this way proved extremely effective in reducing the liquid super-saturation.

The size of the bubbles injected in the water has proven to be a critical factor in determining the effectiveness of gas removal. A very striking result was found by comparing the results of the injection of bubbles at a rate of 4 ml/min and 8 ml/min. The difference between the bubble size distributions in these two cases was essentially limited to bubbles with a radius greater than 150-200 μm , while the absolute numbers of smaller bubbles were comparable in the two cases. The results show that doubling of the gas injection rate in this case has a very small effect on the gas removal rate. This result suggests that the most effective bubbles have a radius of 100 μm or less.

Although very encouraging, our results leave several important questions unanswered for the moment:

1. With the limited means at our disposal we could not study how a scale-up of the nozzle would affect the size of the bubbles generated. Although we were able to generate bubbles with radii in the range of tens of micrometers using a flow passage of a few millimeters squared (a ratio of the order of 1 to 100), in practical applications it would be desirable to use Venturi nozzles with bigger throats. At present, we have no basis to estimate the size of the bubbles that would be generated in this way.
2. Although varying the gas flow rate changed the bubble size distribution, we found that a precise control was difficult to obtain. In particular, increasing the gas flow rate beyond a certain level seemed to only produce many large bubbles, without appreciably increasing the number of the smaller, more effective ones. The role of coalescence in determining this outcome is unclear.
3. The turbulence level in the nozzle must be important in the break-up and coalescence process. It would be very interesting to measure turbulence levels and investigate their effects.
4. The mathematical model that we have developed to interpret the data suggests that, in the right conditions, it is actually easier to remove dissolved nitrogen than dissolved oxygen. This conclusion is very interesting as it is known that nitrogen is the more harmful of the two gases to fish. It would be important to check this conclusion experimentally.

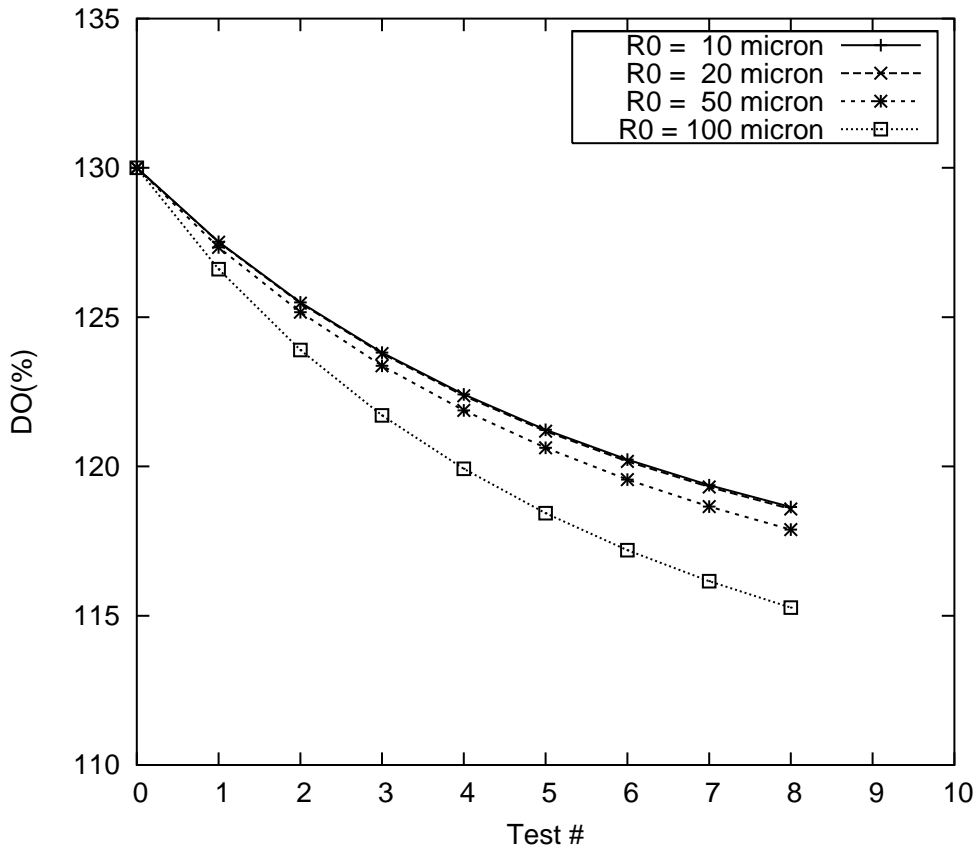


Figure 22: Dissolved oxygen concentration vs. time for bubbles with radii between 10 and 100 μm generated at a constant rate of 110 bubbles/($\text{cm}^2 \text{ s}$); the initial super-saturation is 130% for both oxygen and nitrogen.

5. Cavitation in the nozzle was found to be extremely effective in producing bubbles of a suitable size. Reaching cavitation conditions in the nozzle requires high water velocities and is therefore energetically expensive. It may be that this shortcoming may be offset by the larger number of bubbles generated, especially in a large nozzle. Here again we face a scale-up problem. It may be that the need to run the bubbler for a shorter time may compensate for the increased energy use. On the negative side, cavitation erosion may be a concern.
6. In considering the effect of cavitation, the degree of gas super-saturation is important. If the gas contents is insufficient, the bubbles produced by cavitation may be too small to be effective.

In addition to conducting experiments, we have also developed a mathematical model to describe the evolution of the bubbles over the depth of the tank. The model is one-dimensional and contains many idealizations, but it proves capable of accounting for the experimental observations. In considering possible ways to improve it in future work, several possibilities are immediately apparent:

1. The bubbles induce a recirculating motion in the liquid which is beneficial in that

it promotes surface renewal and therefore a more rapid ex-solution of the gas. Accounting for this feature would require the extension of the model to at least a two-dimensional, or axisymmetric, configuration.

2. An extension along these lines would require the solution of the equations for liquid flow, namely continuity and momentum, properly accounting for the effect of the bubbles on the liquid and of the liquid on the bubbles. A simple way in which this objective could be achieved would be to model the bubbles as point forces applied to the liquid. The bubbles themselves could be assumed to be at their terminal velocity with respect to the local liquid velocity at all times.
3. The rising bubbles cause a state of disordered motion in the liquid sometimes called “pseudo-turbulence”. A model for this effect would probably be important. Although turbulence in two-phase flow is not a well developed area, some simple model along the lines of the $k - \epsilon$ model could be investigated.

References

- BLEVINS, D. 1984 *Applied Fluid Dynamics Handbook*. Van Nostrand.
- CLIFT, R., GRACE, J. & WEBER, M. 1978 *Bubbles, Drops, and Particles*. Academic Press.
- FERRELL, R. T. & HIMMELBLAU, D. M. 1967 Diffusion coefficients of nitrogen and oxygen in water. *J. of Chem. & Eng. Data* **12**, 111–115.
- FUJIWARA, A., WATANABE, K., TAKAGI, S. & MATSUMOTO, Y. 2004 Bubble breakup by pressure wave in bubbly flow. In *3rd International Symposium on Two-Phase Flow Modelling and Experimentation*, pp. Paper No I-143. Pisa, Italy, September 22-24.
- OĞUZ, H. N. 1998 The role of surface disturbances in the entrainment of bubbles by a liquid jet. *J. Fluid Mech.* **372**, 189–212.
- TAKEMURA, F. & YABE, A. 1998 Gas dissolution process of spherical rising gas bubbles. *Chem. Eng. Sci.* **53**, 2691–2699.
- WILHELM, E., BATTINO, R. & WILCOCK, R. J. 1977 Low pressure solubility of gases in liquid water. *Chem. Rev.* **77**, 219–262.